A Cell-type Specific Cortico-subcortical Brain Circuit for Investigatory and Novelty Seeking Behavior

Mehran Ahmadlou[1]*, Janou H.W. Houba[1], Jacqueline F.M. van Vierbergen[1], Maria Giannouli[1], Geoffrey-Alexander Gimenez[1], Christiaan van Weeghel[1], Maryam Darbanfouladi[1], Maryam Yasamin Shirazi[1], Julia Dziubek[1], Mejdy Kacem[1], Fred de Winter[2], J. Alexander Heimel[1]*

[1]Cortical Structure and Function Group, Netherlands Institute for Neuroscience, Meibergdreef 47, 1105 BA Amsterdam, The Netherlands.

[2]Laboratory for Neuroregeneration, Netherlands Institute for Neuroscience, Meibergdreef 47, 1105 BA Amsterdam, The Netherlands.

* Corresponding author. E-mail: m.ahmadlou@nin.knaw.nl, a.heimel@nin.knaw.nl

Exploring the physical and social environment is essential for understanding the surrounding world. We do not know how novelty seeking motivation, initiates the complex sequence of actions that make up investigatory behavior. We found in mice that inhibitory neurons in the medial zona incerta (ZIm), a subthalamic brain region, are essential for the decision to investigate an object or a conspecific. These neurons receive excitatory input from the prelimbic cortex to signal the initiation of exploration. This signal is modulated in the ZIm by the level of investigatory motivation. Increased activity in the ZIm instigates deep investigative action by inhibiting the periaqueductal gray region. Interestingly, a subpopulation of inhibitory ZIm neurons expressing tachykinin 1 (TAC1) modulates the investigatory behavior.

One sentence summary

A subpopulation of inhibitory neurons in the zona incerta drives mice to investigate objects and companions.

Investigating the physical and social environment and novelty seeking behavior is essential for finding new food resources, assessing possible dangers and for better understanding of the surrounding world. Novelty seeking behavior can be dissected into the motivational drive, i.e. curiosity, and the investigatory actions. Curiosity, the motivational drive behind this investigating is considered as intrinsic as hunger and thirst (*1*, *2*). Work on neural mechanisms of curiosity focused on centers involved in reward-prediction in tasks with variable, but immediate, rewards (*3*). Curiosity, however, also drives exploration when there is no expectation of immediate reward, as in the case of novelty seeking behavior (*4*). It is unknown which part of the brain drives this novelty seeking behavior. An area that drives approach and reduces fear in the mouse is the zona incerta (*5–10*). Activity in the rostral zona incerta induces eating (*11*), but activity in the medial zona incerta (ZIm) does not induce consummatory behavior and was reported to induce hunting (*7*, *8*). In mice, however, hunting, foraging and object investigation overlap in both their action sequences (approaching, sniffing, grabbing, biting) and in their modulatory sources such as hunger and stress. This has complicated the analysis and interpretation of the experiments investigating these behaviors and consequently understanding the underlying brain circuits. Lacking double choice tests, it was difficult to determine if the ZIm is involved in investigation, and could be essential in novelty seeking behavior.

To investigate a novel object, mice use a different sequence of actions compared to when they interact with a familiar object.

Mice interact with objects in the surrounding environment for different purposes, such as collecting new information to test edibility or hazardousness. Mice interact less with a familiar object compared to a novel object (*12–14*). However, whether the actions taken to investigate a novel object are different from the actions during interaction with familiar objects is not so clear. Using a free-access double choice (FADC) test (**Fig. 1A and movie S1**), we first tested how mice interact with familiar and novel objects.

The number of approaches and duration of all the actions taken to interact, i.e. sniff, carry, grab, and bite were higher in interaction with the novel object than with the familiar object (**Fig. 1A**). An unsupervised Hidden Markov Model (HMM) showed two states of investigatory behavior: 1. approach and sniff without any other interactions and 2. approach and sniff with further interactions with the highest probability to bite (**fig. S1 A**). Further analysis showed that there was also a much higher probability that after sniffing an object, mice continued their investigation by biting when the object was novel compared to when it was familiar, while none of other transitions was significantly different (**Fig. 1B and fig. S1B**). Our data shows that mice, after sniffing, decide to leave the investigation (with sniff to leave probability of 86% and 65% for familiar and novel objects, respectively) or continue the investigation with other sequences of actions, which mostly start with biting (with sniff to bite probability of 9% and 30% for familiar and novel objects, respectively) (**Fig. 1B and fig. S1B**). Therefore, we categorized the object investigation sequences into shallow investigation (where sniffing is not followed by biting) and deep investigation (where sniffing is followed by biting). In both cases, the investigatory event starts with sniff and ends when no investigatory action (i.e. sniff, bite, grab and carry) is taken anymore for at least 100 ms (**fig. S1 C**). We introduced the deep vs. shallow investigation preference (DSP) using the relative time a mouse carries out deep investigation compared to the shallow investigation. DSP varies between $-\pi/2$ and $\pi/2$, where $-\pi/2$ and $\pi/2$ indicate the absolute preference for shallow and deep investigation, respectively, and 0 indicates equal preference for deep and shallow investigation. This depth of investigation was much higher for novel objects than it was for familiar objects (**Fig. 1C**).

GABAergic neurons in ZIm play a key role in object investigation and modulate its depth.

To investigate whether ZIm plays a role in driving object investigation behavior, we expressed ChR2 by AAV to optogenetically activate inhibitory (GAD2+) neurons in the ZIm (**Fig. 1D and fig. S2A**). Activation of the ZIm^{GAD2} neurons in a 2-minute FADC test with a familiar and a novel object showed an

increase in interaction with novel objects (i.e. sniff, bite, grab and carry) and no significant change in interaction with familiar objects (**Fig. 1E, fig. S2B and movie S2**). Activation of the ZIm^{GAD2} neurons in a more complex FADC test, where we put 4 familiar objects and 1 novel object, gave the same results (**fig. S3, A and B and movie S3**). In novel object investigation compared to familiar object investigation, there was a much higher probability of transition from sniffing to biting, while none of other transitions was significantly different (**fig. S2C**), as in the investigatory sequences of actions in wild-type mice. Furthermore, the DSP in novel object interaction under ChR2 activation was much higher than in tdTOM control mice (**Fig. 1F**), implying that there was a higher increase in deep than in shallow investigation.

To further understand whether the observed increased behavior by activation of the ZIm^{GAD2} neurons is investigatory behavior or food-eating and hunting as well, we used an FADC test with one familiarized food pellet and one novel static object and an FADC with one familiarized living cricket and one novel object moving in parallel with the cricket, respectively. Activation of the ZIm inhibitory neurons in both tests resulted in increased interaction with the novel object compared to the food (**Fig. 1G and movie S4**) or the cricket (**Fig. 1H and movie S5**). Moreover, considering movement and shape/odor/flavor as the main components of the cricket that trigger hunting behavior in mice, we used an FADC test with one novel static object and one familiarized moving object and a FADC with one familiarized immobile cricket (dead). Activation of the ZIm^{GAD2} neurons in both tests showed an increase in the novel object interaction (**fig. S4, B and C**), which again shows that the underlying motivation is to investigate and not to hunt. However, in line with results of a previous study (*11*), activation of the inhibitory neurons in the rostral part of the ZI in an FADC test with one familiarized food and one novel object showed an increase in interaction with the food (binge-like eating) compared to the object (**fig. S5**).

To see whether the ZIm inhibitory neurons are essential in object investigation behavior, we used an AAV virus to express stGtACR2 to suppress the ZIm^{GAD2} neurons (**Fig. 1I and fig. S6A**) in a 10-minute

FADC test with a familiar and a novel object. Suppression of the ZIm^{GAD2} neurons showed no significant change in interactions with the familiar objects (**Fig. 1J and movie S6**). However, in interactions with the novel objects, the number of approaches and duration of sniffing, which is a part of both deep and shallow investigation, stayed unchanged while there was a significant decrease in duration of the investigatory actions that are involved in deep investigation (bite, grab and carry) (**Fig. 1J and fig. S6B**). Furthermore, optogenetic deactivation of the ZIm^{GAD2} neurons decreased the transition probability from sniff to bite when the object was novel (**fig. S6C**) and compared to the tdTOM control mice, showed a lower DSP in the novel object investigation (**Fig. 1K**). Deactivation of ZIm^{GAD2} neurons in a familiar open field arena did not cause a significant change in mobility (**fig. S6D**). Chemogenetically silencing ZIm^{GAD2} neurons (by expressing hM4Di in ZIm^{GAD2} and injecting CNO locally in ZIm) showed the same results, i.e. reduction of the investigation duration and the DSP (**fig. S6, E and F**).

GABAergic neurons in ZIm have a major role in social investigation.

We next asked whether ZIm's role in investigation is specific to objects or if it generalizes to conspecifics, where the actions are different from the actions taken in object investigation. To answer this question, first we used tdTOM control mice in a social investigation test, where we introduced a new conspecific (intruder) (**Fig. 2A**). The first and the last third period of the test were considered as novel and familiar periods, respectively (**Fig. 2A**). The significant reduction of the investigation duration in the familiar period compared to the novel period (**Fig. 2A and fig. S7A**) supports the reduction of novelty in the familiar period. An HMM analysis showed two states of investigatory behavior: 1. approach and investigation without grab and 2. approach and investigation with grab (**fig. S8A**). We calculated the transition probability of approach to investigation without grab (AInv) and approach to investigation with grab (AInvG). The AInvG transition probability showed a significant reduction in the familiar period compared to the novel period, while the AInv transition probability did not show a significant difference.

We categorized the social investigation sequences into shallow investigation (where approach is continued by investigation without grab) and deep investigation (where approach is continued by investigation with grab). In both cases, the investigatory event starts with approach and ends when no investigatory action (i.e. anogenital, facial and body sniffing and grabbing) is taken anymore for at least 100 ms (**fig. S8B**). As before we introduced the deep vs. shallow investigation preference (DSP) using the relative time a mouse carries out deep investigation compared to the time spent in shallow investigation. This depth of investigation was much higher in the novel period than in the familiar period (**Fig. 2C**).

Next, we used AAV virus with ChR2 and stGtACR2 to activate and deactivate ZIm^{GAD2} neurons during the social investigation test. Compared to the tdTOM control mice, activation of the ZIm^{GAD2} neurons in a social investigation test showed a substantial increase in duration of the investigatory interaction with the intruder conspecifics, including the approach/chase, anogenital/body/facial investigation, and grabbing and did not induce any aggressive behavior or biting (**Fig. 2D, fig. S7, B and C and movie S7**). Conversely, deactivation of the ZIm^{GAD2} neurons in the social investigation test showed a significant decrease in duration of the investigatory interaction with the intruder conspecific (**Fig. 2D and fig. S7, B and C**). The DSP in the novel period showed the same results as in the novel object investigation (**Fig. 2E**). Chemogenetically silencing ZIm^{GAD2} neurons (by expressing hM4Di in ZIm^{GAD2} and injecting CNO locally in ZIm) showed the same results, i.e. reduction of the investigation duration and the DSP (**fig. S7, D, E and F**).

ZIm is active during investigation and in high arousal state.

To examine whether inhibitory neurons in the ZIm are naturally active during investigatory behavior, we virally expressed GCaMP6s in the ZIm^{GAD2} neurons and recorded calcium photometry signal from freely moving mice during object and social investigation (**Fig. 3A**). In line with the optogenetic results, the calcium photometry showed a significant activity of ZIm^{GAD2} neurons during both deep ($P < 0.0001$) and

shallow ($P < 0.0001$) investigations and a dramatic increase during deep investigation compared to the shallow investigation (**Fig. 3, B and C and fig. S9 A and B**). While in interaction with the food, the same set of actions as the ones in deep investigation, ZIm^{GAD2} neurons show much less activity than deep investigation (**fig. S9 C**).

It is known that investigatory behavior requires a high arousal level (*15*, *16*), which is confirmed by our pupil measurements using head mounted camera in freely moving mice (**fig. S10**). Therefore, we asked whether activity of ZIm neurons is correlated with the arousal level. We recorded from ZIm units in head-fixed mice using a laminar multichannel electrode during spontaneous arousal changes, which were quantified by the changes in pupil size and whisking. 58% of units in the ZIm were significantly correlated with the arousal level (**Fig. 3D**). We optogenetically activated ZIm^{GAD2} neurons in head-fixed mice and video recorded the pupil and whiskers. These measures revealed that activation of the ZIm^{GAD2} neurons increases the arousal level (**Fig. 3E**). Because curiosity-driven investigation has previously been associated with reward anticipation and positive valence (*17*), we examined whether the increased arousal level coincides with a positive or negative valence. We used a real-time place preference/avoidance test in a double-chamber, where one of the chambers is linked to the optogenetic light (light-chamber). Compared to the tdTOM control mice, activation of ZIm^{GAD2} neurons caused an increase in time spent in the light-chamber (**Fig. 3F**). This result was confirmed by the increase of number of returns to the nose poke linked to the photo-activation of the ZIm^{GAD2} neurons in a self-stimulation task (**fig. S11**).

To examine whether the activation of the ZIm^{GAD2} neurons led to a non-specific and general increase in positive arousal and motivation, or if it specifically induced investigatory behavior, we fasted the mice for 24 hours to induce a strong preference for food-eating (familiar food) compared to the novel object investigation (in an FADC test). The control mice (fasted tdTOM mice) showed a strong preference for

the food (**Fig. 3G**), while activation of ZIm^{GAD2} neurons in the fasted mice dramatically increased the novel object investigation and did not affect the food-eating behavior.

Suppressing prelimbic cortex to ZIm pathway reduces investigatory behavior.

Next, we sought the upstream brain areas to the ZIm involved in the investigatory behavior. We injected a monosynaptic Rabies virus (with a previously injected Cre-dependent helper virus) in the ZIm of GAD2-Cre positive mice. Microscopy revealed several brain areas projecting to the ZIm^{GAD2} neurons, among which Prelimbic Cortex (PL) (**Fig. 4A**) is well established in playing a key role in investigatory behavior (*18*, *19*).

Calcium photometry showed that PL→ZIm axons were active during investigation (deep: $P < 0.0001$; shallow: $P < 0.0001$), but there was no significant difference in their activity during deep and shallow investigations (**Fig. 4, B and C**). Moreover, electrophysiological recordings from PL of head-fixed mice showed that activity of 74% of PL units was significantly correlated with the arousal level (**Fig. 4D**). This raised the question whether the increase in arousal level that we had seen by activation of the ZIm^{GAD2} neurons could be inherited from the PL. To answer this, we first injected AAV-ChR2 in PL of C57BL/6 mice under control of a CaMKII excitatory promoter (**fig. S12, A and B**) (**Fig. 4E**). Photo stimulation of the PL→ZIm axons caused an increase in firing rate of ZIm units (**Fig. 4E**) and a significant increase in pupil size and whisking (**Fig. 4F**).

Then we asked whether the direct projection from PL→ZIm is essential for the investigatory behavior. We expressed hM4Di in PL (and tdtTomato as control) and by local injection of CNO in ZIm, we deactivated the PL→ZIm axons in the FADC object investigation and the social investigation tests. This deactivation of PL→ZIm axons significantly reduced the depth of investigation and suppressed object investigation (**Fig. 4G**) and social investigation (**Fig. 4H**). In vivo electrophysiology confirmed the high efficacy of the local injection of CNO in suppressing the PL input into the ZIm (**Fig. 4I**).

These results imply that the PL input into the ZIm contains a motivational signal, which is essential for investigation. At this processing stage the shallow and deep investigations are not differentiated yet by the size of the signal.

ZIm-PAG projection plays a key role in investigation

To determine the investigatory pathway downstream from the ZIm, we first injected a Cre-dependent AAV tdTOM virus in the ZIm of GAD2-Cre positive mice and found projections of the ZIm^{GAD2} neurons to several downstream brain areas, including the Mesencephalic Locomotor Region (MLR), Pontine Reticular Formation (PnO) and Periaqueductal Gray (PAG) (the lateral divisions: lPAG). Using optogenetics and multichannel extracellular recording in head-fixed mice, we examined to what extent activation of the ZIm^{GAD2} neurons affects the neuronal activity in these brain areas. We observed a significant decrease and increase of activity in portions of units in MLR, PnO and lPAG, with the highest effect on suppressing lPAG units (**Fig. 5A**). To find out to which of these brain areas the inhibitory ZIm projection plays a role in the investigatory behavior, we virally expressed ChR2 in ZIm^{GAD2} neurons and optogenetically activated the axon terminals from ZIm into MLR, PnO and lPAG in the FADC object investigation and the social investigation tests. The behavioral results revealed that activation of the ZIm→lPAG projection significantly increased both novel object investigation (**Fig. 5B**) and social investigation (**Fig. 5C**) (compared to the control tdTOM mice) and that activation of the ZIm→MLR and ZIm→PnO did not have an equally strong effect. Activating the ZIm→lPAG axons also increased the depth of investigation (**fig. S13**). Calcium photometry from GCaMP6s expressed in ZIm→lPAG inhibitory axons showed that these axons were active during investigation. However, they were active only during deep investigation ($p = 0.0014$) and not significantly active during shallow investigation ($p = 0.3876$) (**Fig. 5, D and E**). Moreover, in line with our results from activation of the ZIm^{GAD2} neurons, the activation of the ZIm→lPAG (but not ZIm→MLR and ZIm→PnO) inhibitory projection significantly

increased the arousal level (**fig. S14**). To further understand whether this projection is essential for the investigatory behavior, we first virally expressed hM4Di (and tdTomato as control) in the ZIm^{GAD2} neurons. Then, we injected CNO directly into the lPAG to deactivate the ZIm→lPAG inhibitory projection and half an hour later mice went through the FADC object investigation and the social investigation tests. The deactivation of the ZIm→lPAG inhibitory axons significantly reduced the depth and duration of the object investigation (**Fig. 5F**) and social investigation (**Fig. 5G**).

ZIm inhibitory neurons expressing TAC1 are important for investigation

Diversity of the inhibitory subpopulations in the ZI is one of the reasons underlying the functional diversity of the ZI (*7*, *10*, *20*, *21*). Therefore, we sought to identify the inhibitory subpopulations of ZIm and examined their relevance in the investigatory behavior. Because Tachykinin 1 (TAC1) in some thalamic regions (e.g. in the areas where GABAergic neurons originate from the same lineage cells as the ZI, i.e. thalamic reticular nucleus and lateral geniculate nucleus (*22*)) is exclusively expressed in inhibitory neurons (*23*) (https://portal.brain-map.org/), we examined whether TAC1 is also expressed in ZIm inhibitory neurons. Using double fluorescence in situ hybridization (FISH), we found that the vast majority (92%) of TAC1+ neurons in ZIm are inhibitory and they make up for ~11.5% of the inhibitory (VGAT+) neurons (**Fig. 6, A and B**). Furthermore, multi FISH showed that the TAC1+ population is separate from the previously identified Somatostatin positive (SST+) and Parvalbumin positive (PV+) neuronal populations in the ZIm with less than 2% overlap (**Fig. 6, C and D**). This result was confirmed by immunohistochemistry experiments (**fig. S15C**). TAC1+ neurons are more numerous in the medial part of the ZI than in the rostral and caudal parts (**fig. S15, A and B**).

Next, we optogenetically activated these three inhibitory subpopulations to see which inhibitory cell-type in the ZIm is involved in the investigatory behavior. Activation of PV+ neurons and SST+ neurons during the FADC object investigation and the social investigation tests did not cause a significant change in the

investigatory behavior (**Fig. 6, E and F)**. Although we cannot rule out an effect for PV and SST neurons due to the low sample size, activation of the TAC1+ neurons was different and clearly increased both the object and the social investigation (**Fig. 6, E and F**). Activation of the TAC1+ neurons increased the DSP (**Fig. 6G and fig. S16**) and the level of increase in the investigatory behavior by activating the TAC1+ neurons was not different from that induced by activating the GAD2+ neurons (**fig. S17**). Moreover, activation of the TAC1+ neurons increased the arousal level just as activation of GAD2+ neurons did (**fig. S18**).

Next, by optogenetically deactivating the ZIm^{TAC1} neurons during the FADC object investigation and the social investigation tests, we examined whether the ZIm^{TAC1} neurons are essential for the investigatory behavior. Deactivation of the ZIm^{TAC1} neurons suppressed the investigatory behavior (**Fig. 6H and fig. S13, A and B**). Moreover, retrograde AAV injections in the lPAG (and anterograde AAV injections in the ZIm) and Rabies injections in the ZIm of TAC1-Cre positive mice, respectively, showed that ZIm^{TAC1} neurons project to the lPAG (**Fig. 6J and fig. S15E**) and receive direct input from the PL (**Fig. 6K and fig. S15D** for other inputs), which may explain our behavioral results.

Together, our data demonstrates a brain circuit for driving and gating investigatory motivation and novelty seeking behavior. We showed that using a simple approach of free access double choice, we can distinguish investigatory behavior from food-eating and hunting, providing us with a powerful strategy to study brain circuits underlying investigatory behavior. Using this strategy, together with optogenetics, chemogenetics and calcium fiber photometry, we showed that increasing the ZIm activity increases the motivation to investigate. Cortical excitatory input from PL into ZIm conveys non-specific motivation and arousal level to investigate. Extra information (e.g. sensory inputs from midbrain) and processing selectively multiplies the resulting activity of ZIm^{GAD2} neurons. Next, a thresholding mechanism operates on a subpopulation of ZIm^{GAD2} neurons (likely to be ZIm^{TAC1} neurons), in such a way that only high ZIm

activity causes an inhibitory signal to the PAG leading to deep investigation (**fig. S19**). Although the inhibition of PAG can lead to action by disinhibition of defensive actions within the PAG (*5*, *24*), we argue that the increased exploration is not due to decreased fear, because we found activation of ZIm^{GAD2} increased arousal level and specifically increased deep investigation. However, how the sensory information and motivational signals in ZIm integrate to increase the investigatory motivation and initiate this deep investigation remains to be uncovered. Moreover, as dorsal and ventral subdivisions of ZIm differ in their connectivity and neurochemical composition (*25*, *26*), a further subdivision of function may be discovered.

Methods Summary

Mice were habituated to the experimental box for several days. The object investigation test was implemented using a familiar and a novel object in an FADC manner and for social investigation test mice were exposed to one novel conspecific and the test period was split into the first third and the last third as novel and familiar periods for further analysis. Mice were either wild type with no stimulation or they were optogenetically or chemogenetically stimulated or inhibited during the tests (with the corresponding control groups). HMM and transition probability analyses of the labeled behaviors categorized the investigatory behaviors to shallow and deep investigations and investigation duration and depth of investigation were calculated.

Optogenetic effects on arousal level was measured by pupil size and whisker activity. Anatomical and functional connectivity between ZIm and its inputs and outputs was studied using anterograde and retrograde viruses and in-vivo electrophysiology. Calcium activity of ZIm and its input (PL→ZIm axons) and output (ZIm→lPAG axons) was measured during object and social investigation using fiber photometry. Immunohistochemistry and single-molecule mRNA multi-fluoresent in-situ hybridization was performed to examine ZIm^{TAC1} neurons are a subpopulation of ZIm inhibitory neurons. Furthermore,

we photo-activated and photo-inhibited the ZIm^{TAC1} neurons during object and social investigation tests and measured the effects on investigation duration and depth of investigation.

References and Notes:

1. C. D. Spielberger, L. M. Starr, in *Motivation: Theory and research*, H. F. O'Neill, M. Drillings, Eds. (1994), pp. 221–243.

2. G. Loewenstein, The psychology of curiosity: a review and reinterpretation. *Psychol. Bull.* **116**, 75–98 (1994).

3. C. Kidd, B. Y. Hayden, The Psychology and Neuroscience of Curiosity. *Neuron*. **88**, 449–460 (2015).

4. R. N. Hughes, Neotic preferences in laboratory rodents: Issues, assessment and substrates. *Neurosci. Biobehav. Rev.* **31**, 441–464 (2007).

5. X. L. Chou, X. Wang, Z. G. Zhang, L. Shen, B. Zingg, J. Huang, W. Zhong, L. Mesik, L. I. Zhang, H. W. Tao, Inhibitory gain modulation of defense behaviors by zona incerta. *Nat. Commun.* **9**, 1–12 (2018).

6. M. Zhou, Z. Liu, M. D. Melin, Y. H. Ng, W. Xu, T. C. Südhof, A central amygdala to zona incerta projection is required for acquisition and remote recall of conditioned fear memory. *Nat. Neurosci.* **21**, 1515–1519 (2018).

7. Z. D. Zhao, Z. Chen, X. Xiang, M. Hu, H. Xie, X. Jia, F. Cai, Y. Cui, Z. Chen, L. Qian, J. Liu, C. Shang, Y. Yang, X. Ni, W. Sun, J. Hu, P. Cao, H. Li, W. L. Shen, Zona incerta GABAergic neurons integrate prey-related sensory signals and induce an appetitive drive to promote hunting. *Nat. Neurosci.* **22**, 921–932 (2019).

8. C. Shang, A. Liu, D. Li, Z. Xie, Z. Chen, M. Huang, Y. Li, Y. Wang, W. L. Shen, P. Cao, A subcortical excitatory circuit for sensory-triggered predatory hunting in mice. *Nat. Neurosci.* **22**, 909–920 (2019).

9. A. Venkataraman, N. Brody, P. Reddi, J. Guo, D. G. Rainnie, B. G. Dias, Modulation of fear generalization by the zona incerta. *Proc. Natl. Acad. Sci. U. S. A.* **116**, 9072–9077 (2019).

10. X. Wang, X. Chou, B. Peng, L. Shen, J. J. Huang, L. I. Zhang, H. W. Tao, A cross-modality enhancement of defensive flight via parvalbumin neurons in zonal incerta. *Elife*. **8**, 1–17 (2019).

11. X. Zhang, A. N. Van Den Pol, Rapid binge-like eating and body weight gain driven by zona incerta GABA neuron activation. *Science (80-.).* **356**, 853–859 (2017).

12. E. Dere, J. P. Huston, M. A. De Souza Silva, The pharmacology, neuroanatomy and neurogenetics of one-trial object recognition in rodents. *Neurosci. Biobehav. Rev.* **31**, 673–704 (2007).

13. M. Antunes, G. Biala, The novel object recognition memory: Neurobiology, test procedure, and its modifications. *Cogn. Process.* **13**, 93–110 (2012).

14. A. Ennaceur, J. Delacour, A new one-trial test for neurobiological studies of memory in rats. 1: Behavioral data. *Behav. Brain Res.* **31**, 47–59 (1988).

15. D. E. Berlyne, Curiosity and exploration. *Science (80-.).* **153**, 25–33 (1966).

16. M. T. Bardo, R. L. Donohew, N. G. Harrington, Psychobiology of novelty seeking and drug seeking behavior. *Behav. Brain Res.* **77**, 23–43 (1996).

17. M. J. Kang, M. Hsu, I. M. Krajbich, G. Loewenstein, S. M. McClure, J. T. Y. Wang, C. F. Camerer, The wick in the candle of learning: Epistemic curiosity activates reward circuitry and enhances memory. *Psychol. Sci.* **20**, 963–973 (2009).

18. M. Murugan, H. J. Jang, M. Park, E. M. Miller, J. Cox, J. P. Taliaferro, N. F. Parker, V. Bhave, H. Hur, Y. Liang, A. R. Nectow, J. W. Pillow, I. B. Witten, Combined Social and Spatial Coding in a Descending Projection from the Prefrontal Cortex. *Cell*. **171**, 1663-1677.e16 (2017).

19. B. Liang, L. Zhang, G. Barbera, W. Fang, J. Zhang, X. Chen, R. Chen, Y. Li, D. T. Lin, Distinct and Dynamic ON and OFF Neural Ensembles in the Prefrontal Cortex Code Social Exploration. *Neuron*. **100**, 700-714.e9 (2018).

20. C. Kolmac, J. Mitrofanis, Distribution of various neurochemicals within the zona incerta: An immunocytochemical and histochemical study. *Anat. Embryol. (Berl).* **199**, 265–280 (1999).

21. K. Liu, J. Kim, D. W. Kim, Y. S. Zhang, H. Bao, M. Denaxa, S. A. Lim, E. Kim, C. Liu, I. R. Wickersham, V. Pachinis, S. Hattar, J. Song, S. P. Brown, S. Blackshaw, Lhx6-positive GABA-releasing neurons of the zona incerta promote sleep. *Nature*. **548**, 582–587 (2017).

22. N. Inamura, K. Ono, H. Takebayashi, B. Zalc, K. Ikenaka, Olig2 lineage cells generate gabaergic neurons in the prethalamic nuclei, including the zona incerta, ventral lateral geniculate nucleus and reticular thalamic nucleus. *Dev. Neurosci.* **33**, 118–129 (2011).

23. Y. Li, V. G. Lopez-Huerta, X. Adiconis, K. Levandowski, S. Choi, S. K. Simmons, M. A. Arias-Garcia, B. Guo, A. Y. Yao, T. R. Blosser, R. D. Wimmer, T. Aida, A. Atamian, T. Naik, X. Sun, D. Bi, D. Malhotra, C. C. Hession, R. Shema, M. Gomes, T. Li, E. Hwang, A. Krol, M. Kowalczyk, J. Peça, G. Pan, M. M. Halassa, J. Z. Levin, Z. Fu, G. Feng, Distinct subnetworks of the thalamic reticular nucleus. *Nature*. **583**, 819–824 (2020).

24. P. Tovote, M. S. Esposito, P. Botta, F. Chaudun, J. P. Fadok, M. Markovic, S. B. E. Wolff, C. Ramakrishnan, L. Fenno, K. Deisseroth, C. Herry, S. Arber, A. Lüthi, Midbrain circuits for defensive behaviour. *Nature*. **534**, 206–212 (2016).

25. J. Mitrofanis, Some certainty for the “zone of uncertainty”? Exploring the function of the zona incerta. *Neuroscience*. **130**, 1–15 (2005).

26. C. A. Romanowski, I. J. Mitchell, A. R. Crossman, The organisation of the efferent projections of the zona incerta. *J. Anat.* **143**, 75–95 (1985).

27. A. Heimel, Herseninstituut/Ahmadlou_etal_Science_2021. Zenodo (2021). doi:10.5281/zenodo.4588941

28. H. Taniguchi, M. He, P. Wu, S. Kim, R. Paik, K. Sugino, D. Kvitsani, Y. Fu, J. Lu, Y. Lin, G. Miyoshi, Y. Shima, G. Fishell, S. B. Nelson, Z. J. Huang, A Resource of Cre Driver Lines for Genetic Targeting of GABAergic Neurons in Cerebral Cortex. *Neuron*. **71**, 995–1013 (2011).

29. S. Hippenmeyer, E. Vrieseling, M. Sigrist, T. Portmann, C. Laengle, D. R. Ladle, S. Arber, A developmental switch in the response of DRG neurons to ETS transcription factor signaling. *PLoS Biol.* **3**, 0878–0890 (2005).

30. J. A. Harris, K. E. Hirokawa, S. A. Sorensen, H. Gu, M. Mills, L. L. Ng, P. Bohn, M. Mortrud, B. Ouellette, J. Kidney, K. A. Smith, C. Dang, S. Sunkin, A. Bernard, S. W. Oh, L. Madisen, H. Zeng, Anatomical characterization of Cre driver mice for neural circuit mapping and manipulation. *Front. Neural Circuits*. **8**, 1–16 (2014).

31. J. Mattis, K. M. Tye, E. A. Ferenczi, C. Ramakrishnan, D. J. O'Shea, R. Prakash, L. A. Gunaydin, M. Hyun, L. E. Fenno, V. Gradinaru, O. Yizhar, K. Deisseroth, Principles for applying optogenetic tools derived from direct comparative analysis of microbial opsins. *Nat. Methods.* **9**, 159–172 (2011).

32. N. C. Klapoetke, Y. Murata, S. S. Kim, S. R. Pulver, A. Birdsey-Benson, Y. K. Cho, T. K. Morimoto, A. S. Chuong, E. J. Carpenter, Z. Tian, J. Wang, Y. Xie, Z. Yan, Y. Zhang, B. Y. Chow, B.

Surek, M. Melkonian, V. Jayaraman, M. Constantine-Paton, G. K. Wong, E. S. Boyden, Independent optical excitation of distinct neural populations. *Nat. Methods*, **11**, 338–346 (2014)

33. M. Mahn, L. Gibor, P. Patil, K. Cohen-Kashi Malina, S. Oring, Y. Printz, R. Levy, I. Lampl, O. Yizhar, High-efficiency optogenetic silencing with soma-targeted anion-conducting channelrhodopsins. *Nat. Commun.* **9** (2018), doi:10.1038/s41467-018-06511-8.

34. T.W. Chen, T. J. Wardill, Y. Sun, S. R. Pulver, S. L. Renninger, A. Baohan, E. R. Schreiter, R. A. Kerr, M. B. Orger, V. Jayaraman, L. L. Looger, K. Svoboda, D. S. Kim, Ultrasensitive fluorescent proteins for imaging neuronal activity. *Nature.* **499**, 295-300 (2013)

35. M. Kabra, A. A. Robie, M. Rivera-Alba, S. Branson, K. Branson, JAABA: Interactive machine learning for automatic annotation of animal behavior. *Nat. Methods*. **10**, 64–67 (2013).

36. M. Ahmadlou, J. A. Heimel, Preference for concentric orientations in the mouse superior colliculus. *Nat. Commun.* **6**, 6773 (2015).

37. J. P. Sommeijer, M. Ahmadlou, M. H. Saiepour, K. Seignette, R. Min, J. A. Heimel, C. N. Levelt, Thalamic inhibition regulates critical-period plasticity in visual cortex and thalamus. *Nat. Neurosci.* **20**, 1716–1721 (2017).

38. S. N. Kadir, D. F. M. Goodman, K. D. Harris, High-dimensional cluster analysis with the masked EM algorithm. *Neural Comput.* **26**, 2379–2394 (2014).

39. M. Ahmadlou, L. S. Zweifel, J. A. Heimel, Functional modulation of primary visual cortex by the superior colliculus in the mouse. *Nat. Commun.* **9**, 3895 (2018).

Acknowledgements

We thank Joris Coppens, Andres de Groot, Ralph Hamelink, Maurice Heemskerk, Sonja Hofer, Helmut Kessels, Martin Oomstee, Stephen Super, John van Veldhuijzen, Marian Verhage, Nanneke van der Wal and Joost Verhaagen. **Funding:** This work was supported by Dr. J.L. Dobberke Foundation. F.d.W. was supported by Onderzoekfonds KNAW-instituten, ronde 2019. **Author contributions:** M.A. conceived the study with input from J.A.H. M.A., J.H.W.H., J.F.M.v.V., M.G., G.-A.G, C.v.W., M.D., M.K., M.Y.S. and J.D. collected and analyzed the data. F.d.W. made viral vectors and helped the in situ hybridization. M.A. and J.A.H. wrote the paper. **Competing interests:** Authors declare no competing interests. **Data and materials availability:** All processed data are available at github.org/herseninstituut/Ahmadlou_etal_Science_2021 and at Zenodo (27). Raw movies and scripts are stored on institutional storage and are available upon request from the authors.

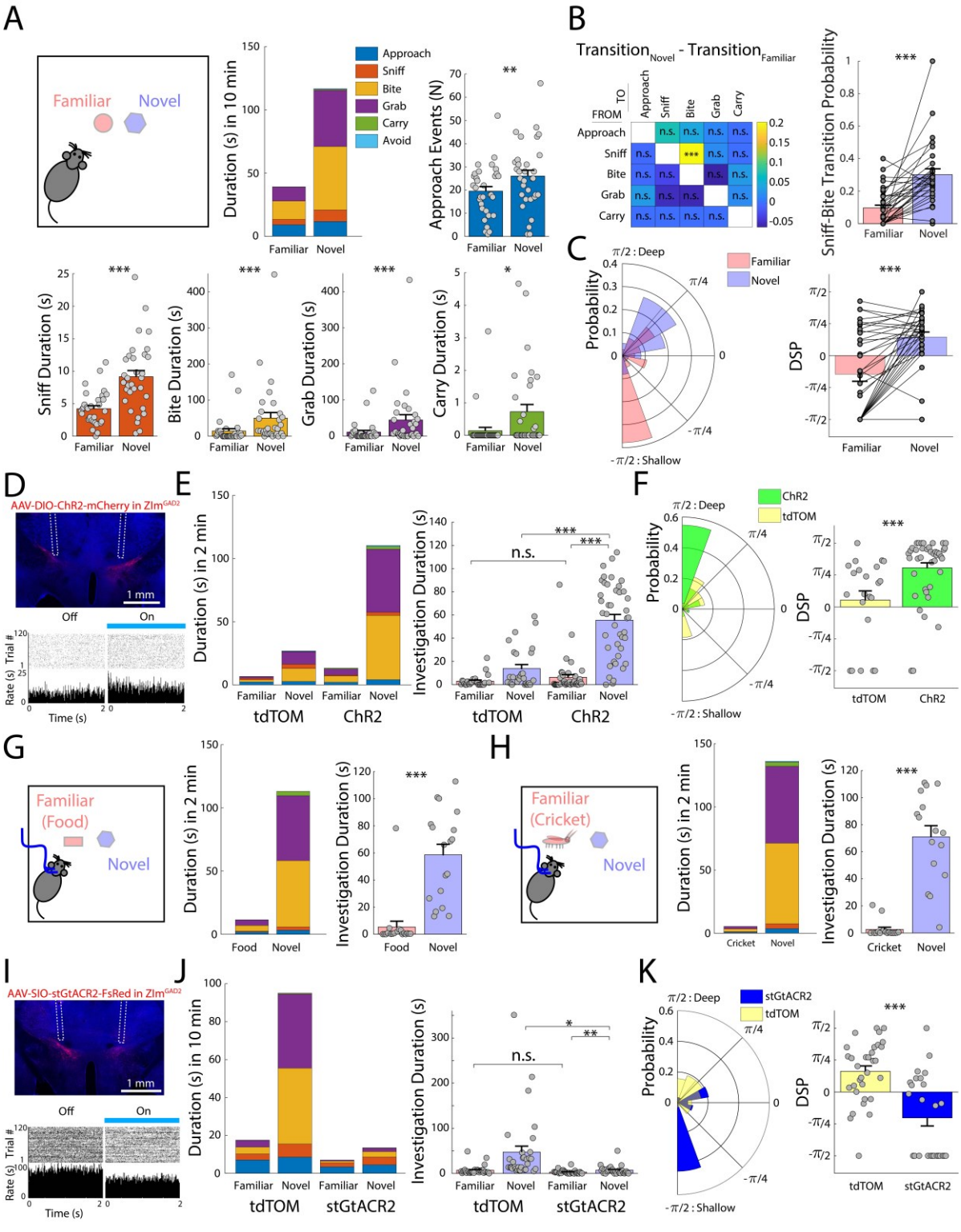
A
Familiar
Novel
Approach
Sniff
Bite
Grab
Carry
Avoid
Duration (s) in 10 min
Approach Events (N)
Sniff Duration (s)
Bite Duration (s)
Grab Duration (s)
Carry Duration (s)
B
Transition Novel - Transition Familiar
TO
FROM
Approach
Sniff
Bite
Grab
Carry
n.s.
Sniff-Bite Transition Probability
C
π/2 : Deep
π/4
0
-π/4
-π/2 : Shallow
Probability
DSP
D
AAV-DIO-ChR2-mCherry in ZIm GAD2
1 mm
Off
On
Trial #
Rate (s)
Time (s)
E
Duration (s) in 2 min
Investigation Duration (s)
tdTOM
ChR2
F
ChR2
tdTOM
G
Familiar (Food)
Novel
Food
H
Familiar (Cricket)
Cricket
I
AAV-SIO-stGtACR2-FsRed in ZIm GAD2
J
stGtACR2
K

Fig 1: Action sequences and role of ZIm GABAergic neurons in object investigation. (**A**) Schematics of an FADC test with familiar and novel objects. Stacked bar graph shows duration for each action (approach, sniff, bite, grab, carry and avoid) taken by C57BL/6 mice to interact with familiar and novel objects averaged over all 10-min tests (n = 37 tests from 8 mice, 4 males). Bar graphs show quantification of individual actions: number of approaches and sniff, carry, grab and bite durations in seconds. (**B**) Representation of the difference between transition matrices of actions taken in novel object and familiar object interactions by the animals in (A). Bar graph shows probability of sniff to bite transition in interaction with familiar and novel objects. (**C**) Probability histogram and bar graph of DSP index of mice in (A) in interaction with familiar and novel objects. DSP varies between $-\pi/2$ and $\pi/2$, where $-\pi/2$ and $\pi/2$ indicate the absolute preference for shallow and deep investigation, respectively, and 0 indicates equal preference for deep and shallow investigation. (**D**) Expression of AAV-ChR2-mCherry in ZIm of a GAD2-Cre mouse and scheme of location of the optic fibers (dashed lines). The lower panel shows an example in-vivo recording of a ZIm neuron with optogenetic light off and on. (**E**) Stacked bar graphs show average duration of actions taken by control mice with tdTomato (n = 27 tests from 4 mice, 2 males) and mice with ChR2-mCherry (n = 42 tests from 7 mice, 4 males) in 2-min FADC tests with familiar and novel objects. Bar graphs show the investigation duration. (**F**) Probability histogram and bar graph of DSP index of mice in (E) in interaction with novel objects. (**G**) Schematics of an FADC test with familiar food and a novel object. The stacked bar graph and the bar graph show duration of the actions and duration of investigation with photoactivation of ZIm^{GAD2} neurons in a 2-min test (n = 16 tests from 7 mice, 4 males). (**H**) Schematics of a FADC with familiar cricket and novel moving object. The stacked bar graph and the bar graph show duration of the actions and duration of investigation with photoactivation of ZIm^{GAD2} neurons in a 2-min test (n = 16 tests from 7 mice, 4 males). (**I**) Example of expression of AAV-stGtACR2-FusionRed in ZIm of a GAD2-Cre mouse and scheme of location of the optic fibers (dashed lines). The lower panel shows an example in-vivo recording of a ZIm neuron with

optogenetic light off and on. (**J**) Stacked bar graphs show average duration of actions taken by control mice with tdTomato (n = 32 tests from 5 mice, 3 males) and mice with stGtACR2-FusionRed (n = 29 tests from 7 mice, 4 males) in 10-min FADC tests with familiar and novel objects. Bar graphs show the investigation duration. (**K**) Probability histogram and bar graph of DSP index of mice in (J) in interaction with novel objects. n.s.: not significant, *: <0.05, **: <0.01 and ***: <0.001.

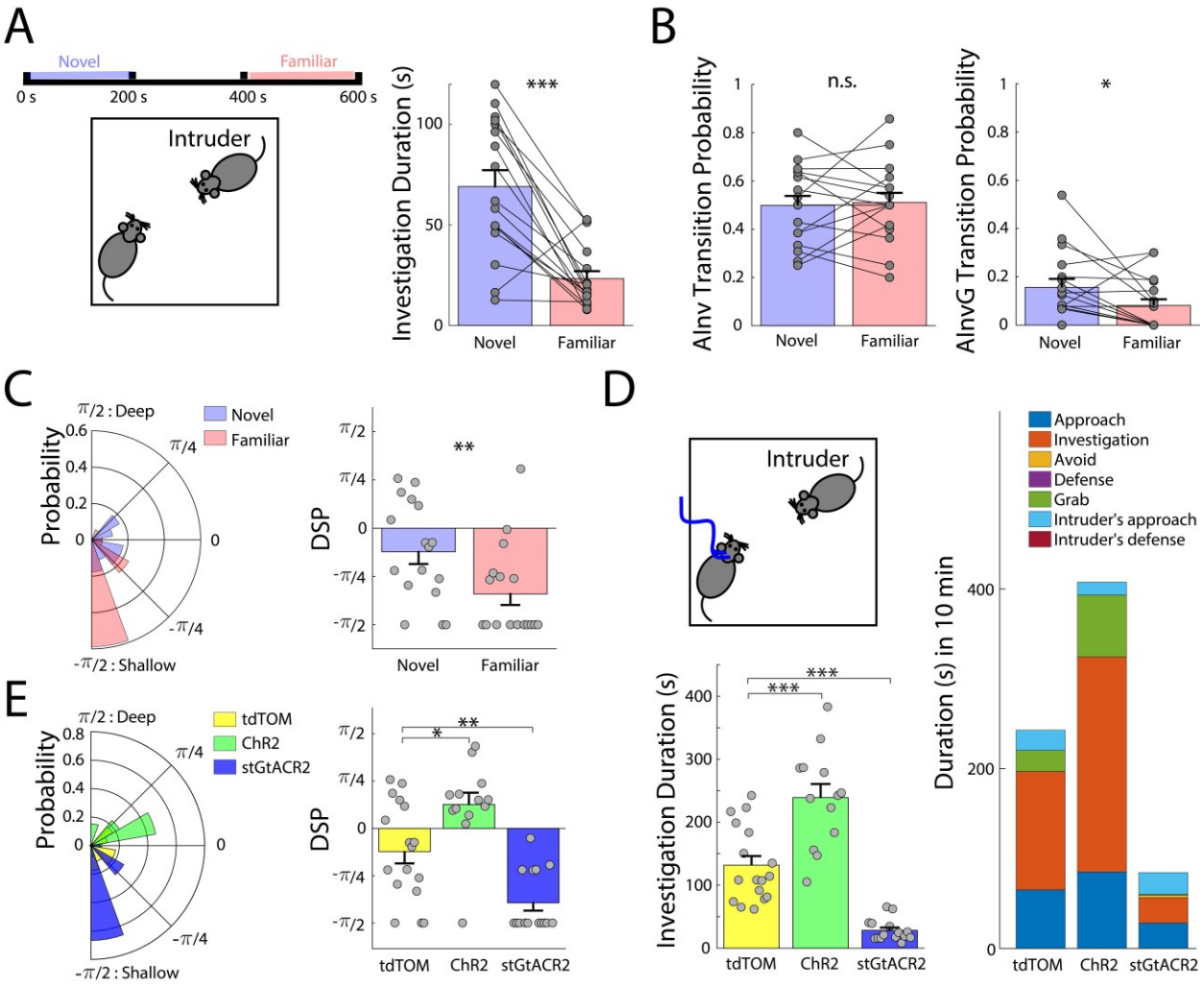

Fig 2: ZIm plays a central role in social investigation. (**A**) Schematics of a 10-min social interaction test, where the first third and the last third of the test are considered novel and familiar periods, respectively. Bar graph shows duration of investigation taken by control tdTomato mice in the familiar and novel periods (n = 17 tests from 8 mice, 4 males). (**B**) Left and right bar graphs show transition from approach to investigation event without grab (AInv) and transition from approach to investigation event with grab (AInvG) in (A), respectively, in the familiar and novel periods. (**C**) Probability histogram and bar graph of DSP index of mice in (A) in familiar and novel periods. (**D**) Schematics shows optogenetic social interaction test. Bar graph shows investigation duration of tdTom (n = 17 tests from 8 mice, 4

males), ChR2 (n = 13 tests from 5 mice, 3 males) and stGtACR2 (n = 15 tests from 6 mice, 3 males) mice in the social interaction test. Stacked bar graph shows duration for each action (approach, investigation, avoid, defense, and grab of the resident mouse, intruder's approach and intruder's defense) taken by the tdTom, ChR2 and stGtACR2 mice. (**E**) Probability histogram and bar graph of DSP index of mice in (D) in the novel period. n.s.: not significant, *: <0.05, **: <0.01 and ***: <0.001.

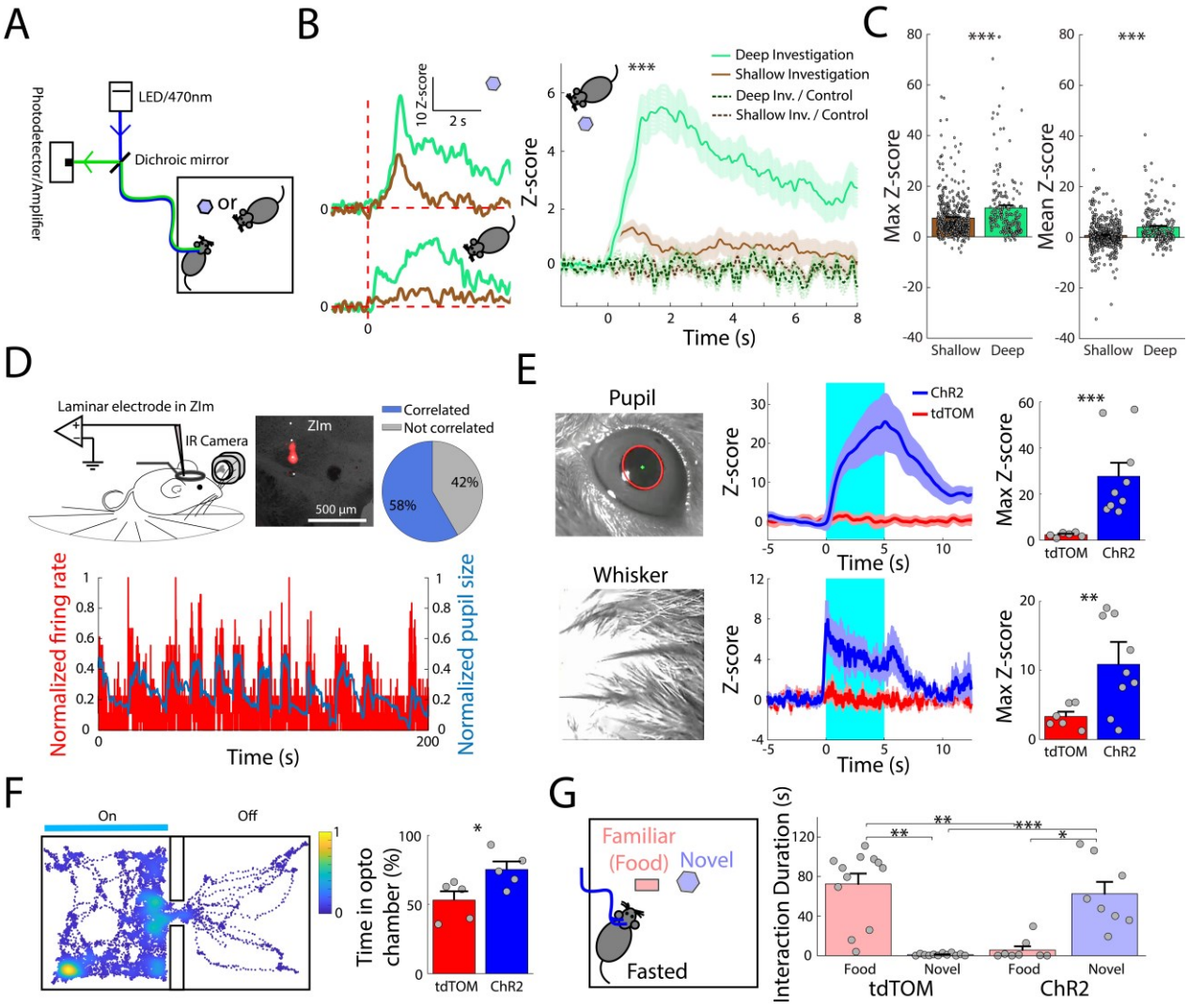

Fig 3: ZIm is active during investigation and in high arousal state. (**A**) Schematics of calcium photometry during social or object interaction. (**B**) Left: Example calcium photometry signals of AAV-GCaMP6s expressing ZIm^{GAD2} neurons during deep (green) and shallow (brown) object investigation (top) and social investigation (bottom). Right: Calcium photometry signals of deep (n = 191 events) and shallow (n = 507 events) investigation averaged over all object and social investigation events (8 mice, 4 males). Signals of control mice with GFP expression in ZIm are represented by dashed lines (n = 58 shallow and deep 91 investigation events from 3 mice, 2 males). Time 0 s indicates start of the

investigation events, i.e. start of sniffing for object investigation and start of approaching the intruder conspecific for social investigation. Dark and the surrounding light colors represent mean±SEM. (**C**) Bar graphs show maximum (left) and mean (right) Z-scores of signals in (B). (**D**) Schematics of extracellular recording of ZIm units with laminar probe and pupil video capturing in awake head-fixed mice. DiI and dashed line show trace of electrode in an example recording from ZIm. Pie diagram shows percentages of the recorded ZIm units that are and are not significantly correlated with the pupil size (n = 173 units from 5 mice, 3 males). Bottom shows normalized pupil size (blue) and normalized firing rate (red) of an example ZIm unit correlated with the pupil size. (**E**) Z-score (middle) and maximum Z-score (right) of pupil size (top) and whisker activity (bottom) of tdTom (red; n = 6 mice, 3 males) and ChR2 (blue; n = 9 mice, 5 males) mice with photo stimulation from 0 to 5 s. (**F**) An example heatmap of the track of a ChR2 mouse in a real time place preference/aversion (RTPPA) test. Bar graph shows duration of time that control tdTom (n = 5 mice, 3 males) and ChR2 (n = 5 mice, 3 males) mice spent in the opto-linked chamber in the RTPPA test. (**G**) Schematics of a fasted mouse in a 2-min FADC test with familiar food and novel object. Bar graph shows duration of time that fasted tdTom (n = 12 tests from 4 mice, 3 males) and fasted ChR2 (n = 8 tests from 6 mice, 4 males) mice interact with the familiar food and the novel object. *: <0.05, **: <0.01 and ***: <0.001.

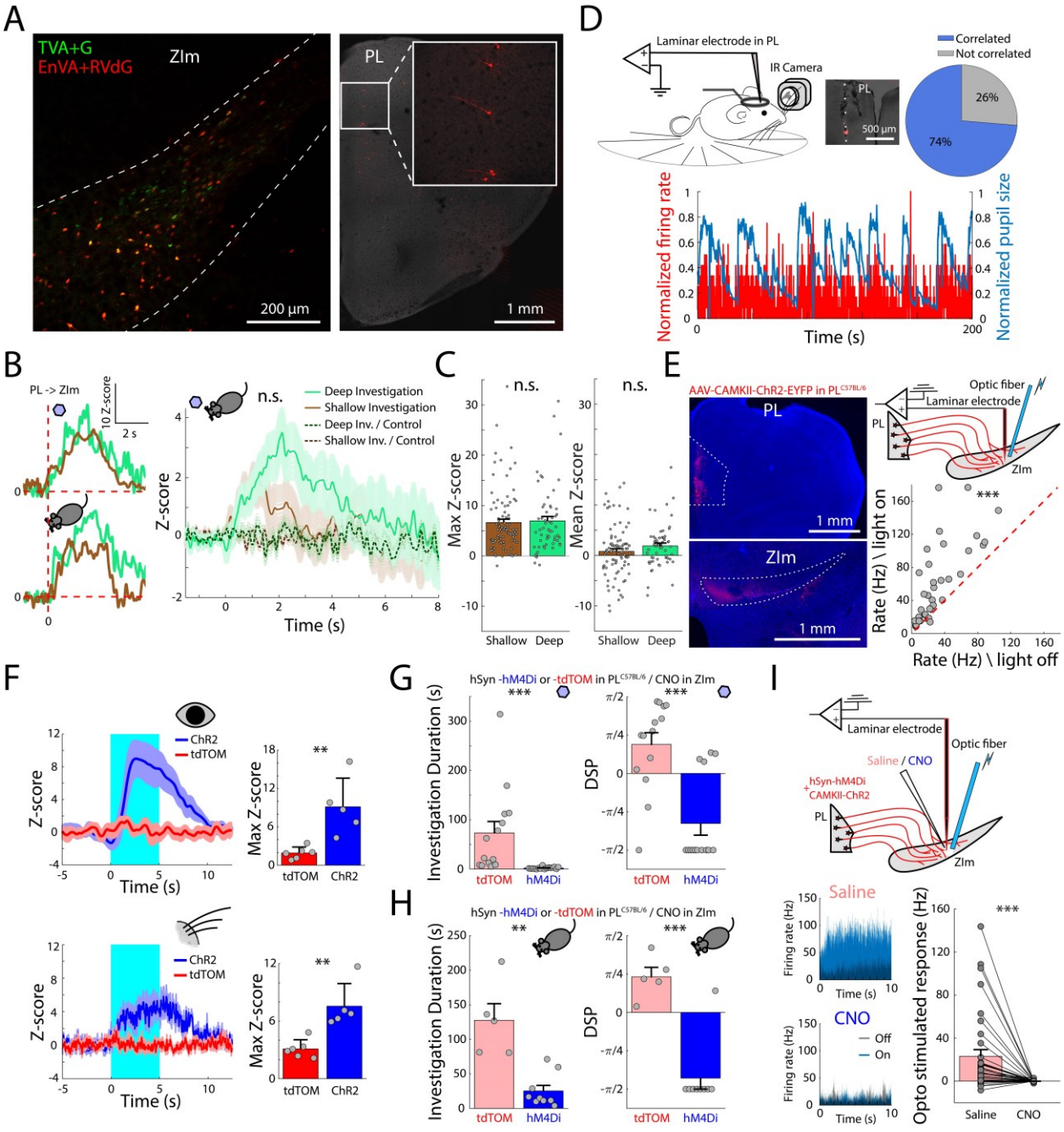

Fig 4: Prelimbic cortex to ZIm pathway is a key factor in investigatory behavior. (**A**) (Left) Retrograde mapping of presynaptic neurons to ZIm^{GAD2} neurons with TVA (GFP) and RVdg (tdTomato). TVA, the avian tumor virus receptor A; G, glycoprotein; EnVA, avian envelope; RVdg, glycoprotein–deleted rabies virus. (Right) Expression of RVdg in ZIm-projecting PL neurons. (**B**) Left: Calcium

photometry signals of PL -> ZIm axons during deep (green) and shallow (brown) object investigation (top) and social investigation (bottom). Right: Calcium photometry signals of deep (n = 57 events) and shallow (n = 90 events) investigation averaged over all object and social investigation events (3 mice, 2 males). Signals of control mice with GFP expression in ZIm are represented by dashed lines. Time 0 s indicates start of the investigation events, i.e. start of sniffing for object investigation and start of approaching the intruder conspecific for social investigation. Dark and the surrounding light colors represent mean±SEM. (**C**) Bar graphs show maximum (left) and mean (right) Z-scores of signals in (B). (**D**) Schematics of extracellular recording of PL units with laminar probe and pupil video capturing in awake head-fixed mice. DiI and dashed line show trace of electrode in an example PL recording. Pie diagram shows percentages of the recorded PL units that are and are not significantly correlated with the pupil size (n = 19 units from 3 mice, 2 males). Bottom shows a normalized pupil size (blue) and normalized firing rate (red) of an example PL unit correlated with the pupil size. (**E**) Left: Expression of AAV-CAMKII-ChR2-EYFP in PL of a C57BL/6 mouse and (Middle) the projections to ZIm. Right: Schematic of in-vivo extracellular recording from ZIm while photo stimulating the PL → ZIm axons (top) and scatter plot of firing rate (Hz) of the ZIm neurons with the optogenetic light above ZIm being on versus off (bottom). (**F**) Z-score (left) and maximum Z-score (right) of pupil size (top) and whisker activity (bottom) of tdTom (red; n = 6 mice, 3 males) and ChR2 (blue; n = 5 mice, 3 males) mice. PL → ZIm axons are photo stimulated from 0 to 5 s. (**G**) Bar graphs show novel object investigation duration (left) and DSP (right) of mice expressing tdTOM (n = 14 tests from 5 mice, 2 males) or hM4Di (n = 16 tests from 5 mice, 2 males) in PL while injecting CNO locally in ZIm. (**H**) Bar graphs show social investigation duration (left) and DSP (right) in the novel period in mice expressing tdTOM (n = 5 tests from 5 mice, 2 males) or hM4Di (n = 9 tests from 5 mice, 2 males) in PL while injecting CNO locally in ZIm. (**I**) Top: schematic of in-vivo extracellular recording from ZIm while photo stimulating the PL → ZIm axons and chemogenetically silencing them by local injection of CNO (top). Bottom left: Firing rate

of an example ZIm neuron in response to photo stimulation of PL → ZIm axons in presence of saline and CNO. Bottom right: bar graph represents responses of ZIm neurons to photo stimulation of PL → ZIm axons in presence of saline and CNO (n = 35 units from 3 mice). n.s.: not significant, *: <0.05, **: <0.01 and ***: <0.001.

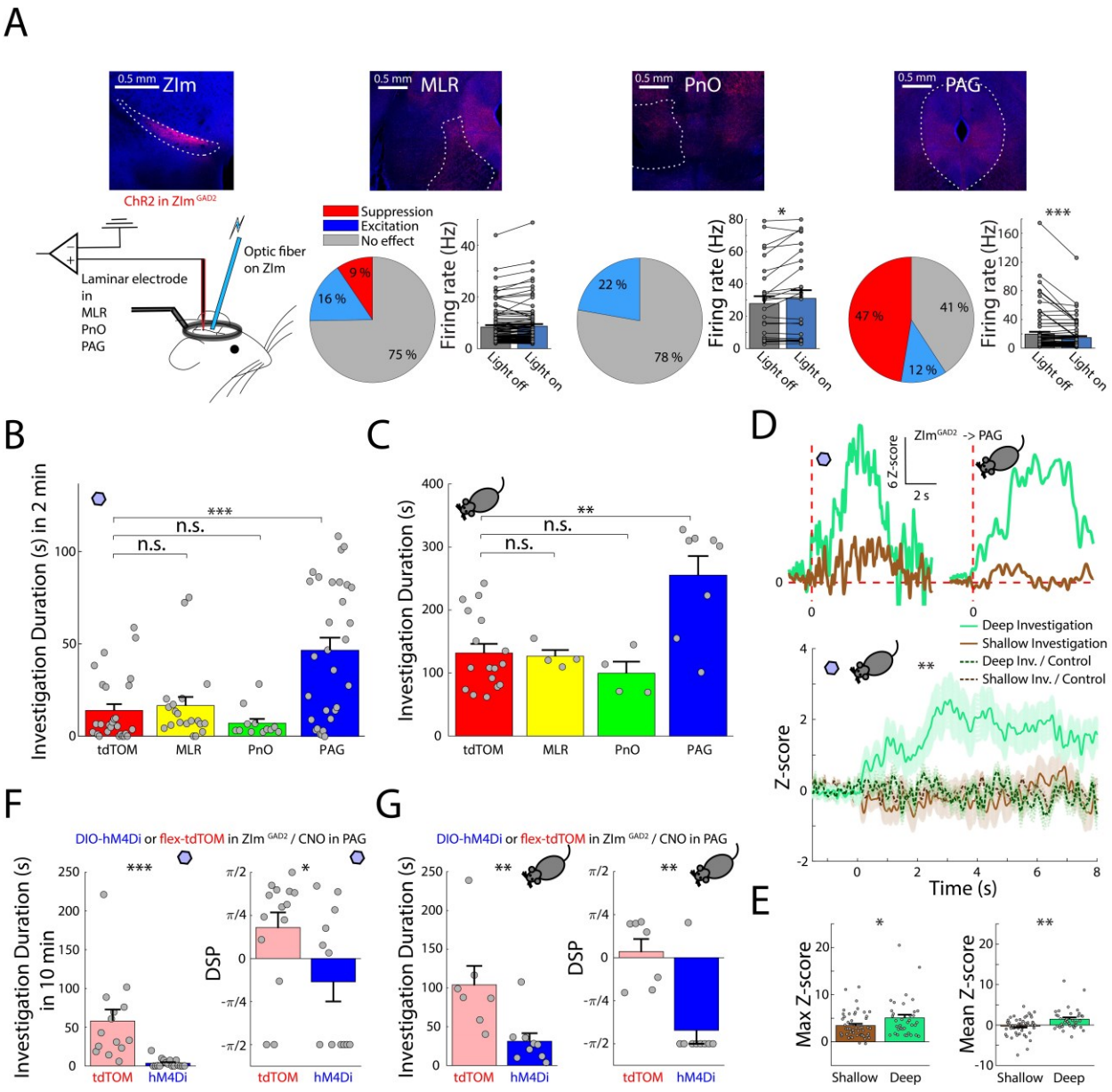

Fig 5: ZIm → PAG projection plays a key role in investigation. (**A**) Expression of AAV-ChR2-mCherry in ZIm^{GAD2} neurons and axons in MLR, PnO and PAG (top; left to right, respectively). The schematics represent the in-vivo experiment of extracellularly recording from ZIm projection targets (MLR, PnO and PAG) while photo stimulating the ZIm^{GAD2}. Pie diagrams show percentage of units in MLR, PnO and PAG (left to right, respectively) that are significantly suppressed (red), excited (blue) or

not changed (gray) by photo stimulation of the ZIm^{GAD2}. Bar graphs show firing rate (Hz) of units in MLR (n = 95 units from 4 mice, 3 males), PnO (n = 27 units from 2 mice, 2 males) and PAG (n = 76 units from 4 mice, 2 males) (left to right, respectively) when photo stimulation light above the ZIm^{GAD2} is off or on. (**B**) Bar graph shows the duration of novel object investigation in control mice with tdTomato (n = 27 tests from 4 mice, 2 males) and mice with ChR2 photo stimulation of ZIm^{GAD2} → MLR (n = 19 tests from 3 mice, 2 males), ZIm^{GAD2} → PnO (n = 12 tests from 3 mice, 2 males) and ZIm^{GAD2} → PAG (n = 30 tests from 5 mice, 3 males) in 2-min FADC tests with familiar and novel objects. (**C**) Bar graph shows the duration of social investigation in control mice with tdTomato (n = 17 tests from 8 mice, 4 males) and mice with ChR2 photo stimulation of ZIm^{GAD2} → MLR (n = 4 tests from 3 mice, 2 males), ZIm^{GAD2} → PnO (n = 4 tests from 3 mice, 2 males) and ZIm^{GAD2} → PAG (n = 8 tests from 5 mice, 3 males). (**D**) Top: example calcium photometry signals of ZIm^{GAD2} → PAG axons during deep (green) and shallow (brown) object investigation (left) and social investigation (right). Bottom: Calcium photometry signals of deep (n = 36 events) and shallow (n = 50 events) investigation averaged over all object and social investigation events (3 mice, 1 male). Signals of control mice with GFP expression in ZIm are represented by dashed lines. Time 0 s indicates the start of the investigation events, i.e. start of sniffing for object investigation and start of approaching the intruder conspecific for social investigation. Dark and the surrounding light colors represent mean±SEM. (**E**) Bar graphs show maximum (left) and mean (right) Z-scores of signals in (D). (**F**) Bar graphs show novel object investigation duration (left) and DSP (right) after injecting CNO locally in PAG of mice expressing tdTOM (n = 14 tests from 5 mice, 3 males) or hM4Di (n = 17 tests from 5 mice, 3 males) in ZIm^{GAD2}. (**G**) Bar graphs show social investigation duration (left) and DSP (right) in the novel period after injecting CNO locally in PAG of mice expressing tdTOM (n = 7 tests from 5 mice, 3 males) or hM4Di (n = 9 tests from 5 mice, 3 males) in ZIm^{GAD2}. n.s.: not significant, *: <0.05, **: <0.01 and ***: <0.001.

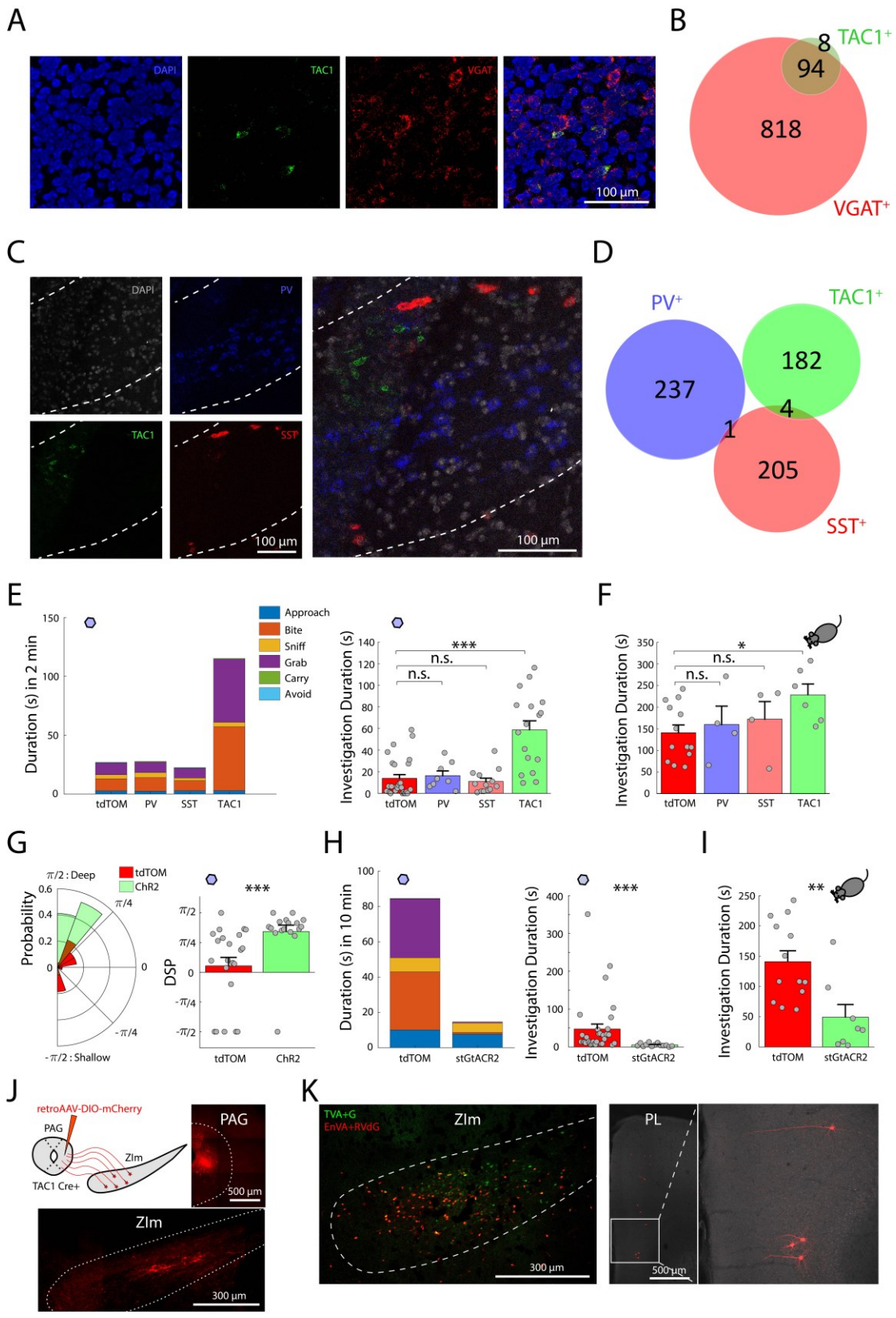
A
DAPI
TAC1
VGAT
100 µm
B
TAC1+
8
94
818
VGAT+
C
DAPI
PV
TAC1
SST
100 µm
100 µm
D
PV+
TAC1+
237
182
4
1
205
SST+
E
Duration (s) in 2 min
Approach
Bite
Sniff
Grab
Carry
Avoid
tdTOM
PV
SST
TAC1
Investigation Duration (s)
***
n.s.
n.s.
F
Investigation Duration (s)
*
n.s.
n.s.
G
π/2 : Deep
tdTOM
ChR2
Probability
-π/2 : Shallow
DSP
***
tdTOM
ChR2
H
Duration (s) in 10 min
tdTOM
stGtACR2
Investigation Duration (s)
***
I
Investigation Duration (s)
**
J
retroAAV-DIO-mCherry
PAG
ZIm
TAC1 Cre+
PAG
500 µm
ZIm
300 µm
K
TVA+G
EnVA+RVdG
ZIm
300 µm
PL
500 µm

Fig 6: The small subpopulation of ZIm inhibitory neurons expressing TAC1 is important for investigation. (**A**) Example of a double-color in-situ mRNA hybridization in ZIm. DAPI is shown in blue and TAC1+ and VGAT+ cells are shown in green and red, respectively. The right shows the overlap between the three colors. (**B**) Venn diagram represents number of TAC1+, VGAT+ and TAC1+/VGAT+ cells in ZIm (from 8 slices). (**C**) Example of a triple-color in-situ mRNA hybridization in ZIm. DAPI is shown in gray and PV+, SST+ and TAC1+ cells are shown in blue, red and green, respectively. The right shows the overlap between the four colors. (**D**) Venn diagram of ZIm cells expressing PV, SST and TAC1 (from 8 slices). (**E**) Stacked bar graphs show average duration of actions taken by control mice with tdTomato (n = 27 tests from 4 mice, 2 males), and mice with ChR2-mCherry expression in ZIm in PV+ neurons (n = 8 tests from 3 mice, 2 males), in SST+ neurons (n = 13 tests from 3 mice, 2 males) and in TAC1+ neurons (n = 17 tests from 5 mice, 3 males) in 2-min FADC tests with familiar and novel objects. Bar graphs represent duration of the novel object investigation. (**F**) Bar graphs represent duration of social investigation in control mice with tdTomato (n = 13 tests from 4 mice, 2 males), and mice with ChR2-mCherry expression in ZIm in PV+ neurons (n = 4 tests from 3 mice, 2 males), in SST+ neurons (n = 4 tests from 3 mice, 2 males) and in TAC1+ neurons (n = 6 tests from 5 mice, 3 males) in social investigation test. (**G**) Probability histogram and bar graph of DSP index of control and TAC1-Cre mice in (E) in interaction with novel objects. (**H**) Stacked bar graph shows average duration of actions taken by control mice with tdTomato (n = 32 tests from 5 mice, 3 males) and mice with stGtACR2-FusionRed expression in ZIm^{TAC1} (n = 13 tests from 5 mice, 3 males) in 10-min FADC tests with familiar and novel objects. Bar graph shows duration of the novel object investigation. (**I**) Bar graph represents duration of social investigation in control mice with tdTomato (n = 13 tests from 4 mice, 2 males) and mice with stGtACR2-FusionRed expression in ZIm^{TAC1} (n = 8 tests from 5 mice, 3 males). (**J**) Schematic of a retrograde tracing experiment with injection of retroAAV-EYFP is PAG of TAC1-Cre mice (n = 2 mice, 2 males) and examples of the EYFP expression in the injection site (PAG) and in the PAG-projecting

ZIm^{TAC1} neurons. (**K**) Left: Rabies monosynaptic retrograde tracing experiment shows the expression of TVA and RVdG in neurons at the injection site (ZIm) in a TAC1-Cre mouse (n = 2 mice, 1 male). Right: expression of RVdG in the PL neurons (right) projecting to ZIm^{TAC1} neurons. n.s.: not significant, *: <0.05, **: <0.01 and ***: <0.001.

List of Supplementary Materials

Materials and Methods

Figs. S1 to S20

Tables S1 to S2

Movies S1 to S7

References only cited in Supplementary Materials (*28–39*).

Supplementary Materials for

A Cell-type Specific Cortico-subcortical Brain Circuit for Curiosity and Novelty Seeking Behavior

Mehran Ahmadlou*, Janou H.W. Houba, Jacqueline F.M. van Vierbergen, Maria Giannouli, Geoffrey-Alexander Gimenez, Christiaan van Weeghel, Maryam Darbanfouladi, Maryam Yasamin Shirazi, Julia Dziubek, Mejdy Kacem, Fred de Winter, J. Alexander Heimel*

* Corresponding author. E-mail: m.ahmadlou@nin.knaw.nl, a.heimel@nin.knaw.nl

This PDF file includes:

Other Suplementary Materials for this manuscript includes the following:

Materials and Methods

Animals

Mice were housed under controlled climate (22-24 ºC) in a normal light/dark cycle (12 hr / 12 hr) with ad libitum access to laboratory food pellets and water. C57BL/6J (Janvier) mice and Gad2-Cre (Stock #028867, Jackson) (*28*), PV-Cre (Stock #017320, Jackson), (*29*), SST-Cre (Stock # 028864, Jackson), (*28*) and TAC1-Cre (Stock #021877, Jackson), (*30*) mice of 2–5 months of age from either sex were used for the experiments. Exact number of males and females is mentioned in the captions of figures. All experimental protocols were approved by institutional animal care and use committee of the Royal Netherlands Academy of Sciences (KNAW) and were in accordance with the Dutch Law on Animal Experimentation. Reporting has followed ARRIVE guidelines.

Virus vector injection

Mice were anesthetized with isoflurane (5% induction, 1.2–1.8% maintenance) in oxygen (0.6 L per min flow rate). Body temperature was maintained at 36.5 ℃, using a controlled heating pad (Harvard Apparatus). The eyes were protected from light by black stickers and from drying by Cavasan eye ointment. During their surgery, mice were administered the analgesic Metacam (1 mg per kg s.c.) to reduce pain during the recovery. Using ear bars, mice were head fixed on a stereotactic device (Kopf) and using a scalpel blade the scalp along with the midline was cut to expose the skull. Small craniotomies were made by dental drill and using a Drummond Nanoject volume injector the virus was injected into the target brain regions. Fifteen minutes after the injection, the glass pipette was retracted and in case we did not need fiber implantation, the scalp was sutured. After recovery, the animals were returned to their cage.

Brain regions and coordinates (from Bregma) used for virus injections: ZIm (AP: -1.8 mm, ML: 1.0 mm, DV: 4.4 mm), PAG (AP: -4.5 mm, ML: 0.5 mm, DV: 2.2-2.6 mm), PL (AP: +1.9 mm, ML: 0.4 mm, DV: 2.0-2.2 mm) and ZIr (AP: -1.0 mm, ML: 1.0 mm, DV: 4.4 mm). For optogenetic experiments, we used AAV9-hEF1a-DIO-mCherry-hChR2 (University of Zurich; V80-9, a gift from Karl Deisseroth), AAV9-CaMKII-EYFP-hChR2 (*31*) (Addgene viral prep #35505, a gift from Karl Deisseroth), AAV5-Syn-FLEX-tdTomato-ChrimsonR (*32*) (Addgene viral prep #62723-AAV5, a gift from Edward Boyden), AAV1-hSyn-SIO-FusionRed-stGtACR2 (*33*); Addgene viral prep #105677-AAV1, a gift from Ofer Yizhar) and AAV9-hSyn-FLEX-tdTomato (made in the host institute), for chemogenetic experiments, AAV8-hSyn-mCherry-hM4Di (Addgene viral prep #50475-AAV8, a gift from Bryan Roth) and AAV1-hSyn-DIO-mCherry-hM4Di (made in the host institute), for fiberphotometry experiments, AAV1-Syn-FLEX-GCaMP6s (*34*) (University of Pennsylvania, a gift from Douglas Kim & GENIE Project), AAV9-Syn-GCaMP6s-WPRE-SV40 (*34*) (University of Pennsylvania, a gift from Douglas Kim & GENIE Project) and AAV9-hSyn-EGFP (made in the host institute) and for tracing experiments, retroAAV-EF1a-DIO-hChR2-mCherry (Addgene viral prep #20297-AAVrg), AAV1-hSyn-FLEX-TVA-p2A-EGFP-2A-oG (Salk Institute, a gift from John Naughton) and G-deleted Rabies-EnvA-mCherry (Salk Institute, a gift from Edward Callaway).

For Rabies virus tracing, we first injected the helper virus (AAV1-hSyn-FLEX-TVA-p2A-EGFP-2A-oG) in the target brain region (80 nl) and after 3 weeks we injected

the Rabies (G-deleted Rabies-EnvA-mCherry) in the same location (40 nl). Seven days after the Rabies injection, mice were transcardially perfused for confocal microscopy (Leica, SP5).

Optic fiber implantation

For optogenetic behavior tests and fiber photometry, mice were fiber implanted during the virus injection surgery. After the virus injection, the scalp and soft tissue overlying the skull were incised to expose the skull. Craniotomies with 300-400 µm diameter were made (by dental drill) to insert the optic fibers (200 µm diameter). After cementing a metal ring (9 mm inner diameter) to the skull, the optic fibers were inserted 100 µm (for optogenetics; N.A.: 0.39) or 50 µm (for fiber photometry; N.A.: 0.50) above the target brain regions and cemented to the skull. After recovery, the animals were returned to their cage. Positions and coordinates (from Bregma) used for optic fiber implantation: ZIm (AP: -1.8 mm, ML: 1.2 mm, angle: 2.5^{o}), PAG (AP: -4.5 mm, ML: 1.2 mm, angle: 18^{o}), MLR (AP: -4.7 mm, ML: 1.3 mm, angle: 2^{o}), PnO (AP: -4.4 mm, ML: 1.3 mm, angle: 6^{o}) and ZIr (AP: -1.0 mm, ML: 1.2 mm, angle: 2.5^{o}).

Behavior tests and analysis

Mice were habituated to the experimenters and the experimental box (35 cm × 35 cm × 35 cm) every day for three weeks. For object investigation tests, mice were also habituated to one object in the box and one alive cricket (Acheta domesticus, size 6, Kreca Ento-Feed) every day for the last three days before the experiment. Object investigation tests were designed in a free access double choice manner. Mice were put in the box for 30 min before the experiment with an object in the last 10 minutes. Then a novel object (randomly assigned among 30 objects with different shapes, colors, textures and materials; **Fig. S20**) was put together with the familiar object for 2 min or 10 min with photo-stimulation or photo-inhibition, respectively. The reason to use 10 minute experiments for wild type mice was that 2 minutes is too short to have sufficient investigatory actions. Without 10 minutes tests, we could not collect and quantify details of behavior and investigate the sequences. Therefore, we kept the experiments 10 minutes long unless where we used photo-stimulation. In the case of photo-stimulation, the test lasted 2 minutes and a control group of 2 minutes was used as well. Wherever we have used 2 minutes test and 10 minutes test we have mentioned it both in the caption and in the figure. Moreover, when we clip the 10 minutes data of photo-inhibition and the corresponding controls into 2 minutes, the results stay the same.

All objects were small (length between 1.0-1.5 cm) and light enough for the mice to be able to pick up and displace. The behavior was video recorded. Objects were left in the box for 10 minutes after the test. Then a new test started by removing the previous familiar object and adding a novel object. Therefore, we considered an object to be a familiar object if it had been introduced to the mouse within the last 10 min. Where it is mentioned, we have put four familiar objects and one novel object. For tests with live crickets or food, first, the cricket or food pellet was put in the box for 10 min and then a novel object was introduced for the test. For object investigation tests with food deprivation, mice were food fasted 24 hours before the test. For social investigation tests, the conspecific intruder (with the same sex and weight (± 1 grams)) was placed in the box after the mouse had been there for 30 min. The same pairs never repeated the test. The

intruder was always a new mouse for the 'resident' mouse that had been in the box. The behavior was video recorded for 10 min. For both object and social investigation tests, the photo activation was done by laser (465 nm; 3 mW at the tip of the optic fiber; Shanghai Laser & Optics Century Co.) switching at 20 Hz with 50% duty cycle and the photo inhibition was done by laser (465 nm; 3 mW at the tip of the optic fiber) shining continuously (0 Hz) throughout the test duration. In case we needed to silence hM4Di-expressed axon terminals (or tdTomato-expressed axons as control), we locally injected 100 nl of CNO-dihydrochloride (10 μM) in the target region 30 minutes before the test, using a Drummond Nanoject volume injector.

Videos of the trials were labeled frame by frame using JAABA (*35*). Analyzers were blind to the experimental groups of the mice. The behaviors displayed during object interaction were categorized as: approaching (turning of the head towards the object accompanied by a body movement decreasing the distance between the mouse and the object; approaches were only counted when the mouse started more than 0.5 cm from the object and ended when the mouse was at 0.5 cm of the object; The body point for distance thresholding was the nose tip. The head direction was considered to be towards the object if the imaginary line between head center and nose tip was aligned with object.), sniffing (being within whisking distance of the object (closer than 0.5 cm) and facing the object, seemingly paying attention to it, mouse can poke the object but explicitly not biting it), biting (taking hold of the object between its jaws and/or making nibbling motions with its head, but explicitly not walking around with it), grabbing (holding of the object between the front paws, or standing over the object and blocking the object, effectively preventing it from moving away), carrying (holding the object in its mouth and simultaneously walking around the box with it, effectively displacing the object), and avoiding (initially facing the object, abruptly moving away from it, increasing the distance between itself and the object. This was labeled from the onset of the sudden movement until ceasing of movement or when the mouse was no longer increasing its distance relative to the object). These actions could occur simultaneously and overlap in time. The behaviors displayed during social interaction were categorized as: approach (turning of the head towards the intruder accompanied by a body movement decreasing the distance between itself and the intruder. Following/pursuing intruder is also included: in case the intruder does not move, the approach ends when the mouse nose reaches 0.5 cm distance from any part of the intruder), investigation (including body investigation, facial investigation, anogenital investigation and grabbing/holding the intruder), grab (holding the intruder with the front paws or standing on it, seemingly to prevent it from moving away), avoid (abruptly moving away from the intruder and increasing the distance between itself and the intruder. This was labeled from the onset of the sudden movement until ceasing of movement or when the mouse was no longer trying to increase its distance to the intruder), defense (defending itself from the intruder, fighting, jumping), intruder's approach (approaching of the intruder towards the mouse) and intruder's defense. The JAABA labeling was imported to MATLAB for further analysis (using custom-written MATLAB programs).

To create a Hidden Markov Model (HMM) we needed an estimated transition matrix, an estimated emission matrix and a sequence as input. The sequence was generated with the data from the 10-min social interaction videos or 10-min object interaction videos, previously analyzed in JAABA. We created a non-overlapping

sequence, with just one action happening at each time. For social interaction analysis, we did this by creating a ranking sequence in which non-investigatory behavior was the lowest, then approach of conspecific intruder, approach by the mouse, investigation and grabbing was the highest rank, and picked the highest rank as current action. For object interaction analysis, we did this by creating a ranking sequence in which non-investigatory behavior was the lowest, then approach, sniffing, carrying, grabbing and biting was the highest rank, and picked the highest rank as current action. We assumed that the higher the rank was, the more important information it conveyed of the mice's state for investigatory behavior. The reason to choose the biting as the highest rank was that the transition probability from sniff to bite is much higher in novel object interactions compare to familiar object interactions, and no other transition probability between actions was significantly different (**Fig. 1B**). In this model, we wanted to focus on the presence of the different states and their relation to each other. We thus squeezed the duration of each action into one time-bin, such that each action only comprises one rank-number for that specific event. The sequence of each movie was put into one vector. We made set the initial settings to three states, because we hypothesized that there would be three underlying states in the behavior, no interest to investigate, little interest to investigate and high interest to investigate. Since we did not have a priori information on the transitions between the states, our starting estimate for the transition matrix contained equal probabilities for all transitions. We generated the initial estimated emission matrix by predicting the likelihood of a behavior present in a certain state. Finally, we used the built-in HMM function hmmtrain and hmmviterbi in MATLAB to get the transition and emissions matrices.

Based on HMM results and the difference between the transition matrices of novel and familiar objects in the object investigation tests (**Fig. 1**), deep investigation and shallow investigation was defined: the object investigation sequences were categorized into shallow investigation (where sniff is not continued by bite) and deep investigation (where sniff is continued by bite). In both cases, the investigatory event starts with sniff and ends when there is no investigatory action (i.e. sniff, bite, grab and carry) is taken anymore for at least 100 ms. Based on HMM results (**Fig. 2**), social investigation sequences were categorized into shallow investigation (where approach is continued by investigation without grab) and deep investigation (where approach is continued by investigation with grab). In both cases, the investigatory event starts with approach and ends when there is no investigatory action (i.e. anogenital, facial and body sniffing and grabbing) is taken anymore for at least 100 ms.

For every investigation test, T_{Deep} and T_{Shallow} were calculated as the sum of the durations of all deep investigation and shallow investigation sequences, respectively. We introduced the relative time the mouse does deep investigation compared to the shallow investigation, as the deep vs. shallow investigation preference (DSP):

$$DSP = \sin^{-1}\left(\frac{T_{\text{Deep}} - T_{\text{Shallow}}}{T_{\text{Deep}} + T_{\text{Shallow}}}\right)$$

This index serves as a ratio between time spent in deep investigation and shallow investigation, expressed as an angle. The DSP ranges from -π/2 to π/2 rad, with -π/2 rad meaning the mouse exclusively displayed shallow investigation, π/2 rad meaning that the mouse exclusively displayed deep investigation, and 0 rad meaning equal preference for deep and shallow investigation.

Calcium fiber photometry and data analysis

Mice were habituated to the experimenters and the experimental box (35 cm × 35 cm × 35 cm) every day for three weeks. At least 3 weeks after the GCaMP6 viral injection and the optic fiber implantation, calcium activity of the target regions were recorded by a fiber photometry system (Doric Lenses) in freely moving mice in interactions with novel objects, food pellets and conspecifics. The behavior movies and calcium transients or control EGFP signals were recorded simultaneously using Raspberry Pi cameras (frame rate: 30 fps) and the fiber photometry system (sampling rate: 100 Hz), respectively. The excitation blue light (LED; 465 nm) at the tip of the optic fiber (N.A.: 0.50) was adjusted around 30 µW. The data for fiber photometry was analyzed using a custom-written MATLAB program. Behavior of the mouse and deep and shallow investigation events were analyzed using JAABA, similarly to the optogenetic experiments. Onset of the behavior labels was considered as time zero to calculate the values of calcium transients change (Z-score): onset of sniff for object investigation and onset of approach for social investigation. These onsets are based on the previously defined deep and shallow investigations. The baseline was taken 1.5 seconds prior to the start of each investigation event. Z-score was calculated by subtracting the mean baseline and further dividing by the standard deviation of the baseline distribution. Behavior of the mouse in interaction with food pellets was analyzed using JAABA, similarly to the object interaction labeling (i.e. approach, sniff, bite, grab and carry). Consequently, deep-like (sniffing food followed by biting) and shallow-like (sniffing food not followed by biting) interaction events with food were computed the same way as deep and shallow object investigation event.

Electrophysiology surgery and in-vivo recording

Mice were anesthetized with isoflurane (5% induction, 1.2–1.8% maintenance) in oxygen (0.6 L per min flow rate). Body temperature was maintained at 36.5 ℃, using a controlled heating pad. The eyes were protected from light by black stickers and from drying by Cavasan eye ointment. During their surgery, mice were administered the analgesic Metacam (1 mg/kg s.c.) to reduce pain during the recovery. Mice were head fixed on a stereotactic device (Kopf) and the scalp and soft tissue overlying the skull were incised to expose the skull. A metal ring (9 mm inner diameter) was attached to the skull with dental cement. Small craniotomies for recording were made by dental drill and the skull was covered by Kwik-Cast Silicone Sealant (World Precision Instruments). After recovery, the animals were returned to their cage. Mice were habituated to being head-fixed to a magnet on the experimental setup (a running disk) 1 hr a day for one week. Then, using a 16-channel micro-electrode (50 µm channel-distance; Neuronexus) and a multi-channel recording system (Tucker-Davis Technologies), the target brain regions were recorded. In case we needed to investigate an optogenetic effect, we inserted an optic fiber (200 µm diameter; N.A.: 0.39) 50 µm above the recorded region. In case we needed to monitor the arousal level, we captured pupil and whisker movies using an IR camera (Basler acA640-90um) during the electrophysiological recordings. In case we needed to silence hM4Di-expressed axon terminals, we locally injected 100 nl of CNO-dihydrochloride (10 µM) in the target region (with saline injection as control), using a Drummond Nanoject volume injector. Animals were killed at the end of the

recording session by an overdose of pentobarbital (100 mg/kg i.p.) and transcardially perfused for histology.

Electrophysiology data analysis

Laminar probe signals were amplified and filtered at 500 Hz–10 kHz and digitized at 24 kHz using RX5 pentusa (Tucker-Davis Technologies). The electrophysiology analysis was done using a homemade MATLAB toolbox, InVivoTools (https://github.com/heimel/InVivoTools) (*36*, *37*). Signals were thresholded at 3x standard deviation to isolate spikes, and spikes were sorted in a multidimensional space of temporal and morphological features of waveforms by custom-written MATLAB scripts using Klustakwik (*38*) and a custom-written Principle Component Analysis (PCA) based method (a part of InVivoTools) (*39*). Single and multi-units were pooled together for this study.

Pupil size, whisker activity and data analysis

For these experiments, mice were habituated for one week (1 hr a day) to the head-fixed setup. At least 3 weeks after the virus injection/fiber implantation surgery, mice with expression of tdTomato (control) or ChR2 in the target brain regions were used for measuring physiological arousal level change by Photostimulation in a room with dim ambient (scattered) light (illuminance: ~20 lux). Mice were head-fixed using a magnet and an infrared LED light was directed to the face (mounted 10 cm away). The implanted fibers (N.A.: 0.39) were coupled to a 465 nm laser (3 mW at the tip of the optic fiber). Mice received 20 Hz photostimulation (with 50% duty cycle) with 5 s pulses (20 pulses with 15 s intervals). We monitored the effect of photostimulation on the arousal level by recording pupil and whisker movies (IR camera: Basler acA640-90um; with frame rate of 25 fps). Whisker activity of each frame was calculated by absolute value of subtraction of the averaged intensity of that frame from the previous frame. The pupil size and whisker activity data were measured using a custom-written MATLAB program.

Real-time place preference/avoidance test

At least 3 weeks after the virus injection/fiber implantation surgery, mice with expression of ChR2 or tdTomato (control) in ZIm^{GAD2} were used for Real-time place preference/avoidance test in a two-chamber white box (60 cm × 30 cm × 30 cm) without additional contextual cues. After 10 min habituation to the box, one chamber was paired with a 20 Hz photostimulation and the other identical chamber had no photostimulation. The laser-coupled chamber was randomly assigned. Total test duration was 10 min. Mice tracks were analyzed using Bonsai software (https://open-ephys.org/bonsai).

Head mounted camera in freely moving mice

For pupil diameter measurements of investigation in freely moving mice, we first cemented a headplate to the skull (under isoflurane anaesthesia) using the procedure that was also used for fiber implants. A miniature camera (SMTKEY mini 600TVL) and mini infrared LED could be temporarily mounted to this headplate using a custom-made bracket and a weight-balancing pulley system. First, the mice were habituated in two sessions to wearing the camera in an observation box with a dim ceiling light (illuminance: ~30 lux). For the recording session, one or more small objects were placed

in the box with the mouse. The 25 frames-per-second videostream from the head camera was digitized by a Terratec 10620 USB video grabber. The pupil diameter was estimated automatically for each frame by custom-made matlab scripts (available on github.com/heimel/InVivoTools) followed by manual curation. The pupil diameter could occasionally not be accurately determined in a frame due to movement noise or other artefacts. For this reason, the pupil diameter and areas were computed as moving medians over 1 s of the pupil measurements in the individual frames. Periods of imaging in which the mean squared error of the frame-by-frame pupil diameter to this moving median was higher than 250 square pixels were excluded from further analysis. For the analysis, we included all other events of deep investigation that were not preceded in the 10 s before the onset of the investigation by an encounter with an object. Start of deep investigation was the onset of sniffing the objects.

Self-stimulation nose poke test

Mice with expression of ChR2 or tdTomato (control) in ZIm^{GAD2} were habituated to the experimental box (35 cm × 30 cm × 35 cm; l × w × h) with a two-port nose-poke system for the last three days before the test (1 hour per day). During the habituation period, drops of 10% sucrose water were delivered through both ports to habituate the mice to the nose poke ports. For the test, there was no sucrose water delivery. During the test, an infrared sensor in one nose poke port led to photo stimulation (20 Hz, 3 mW at the tip of the optic fiber, 50% duty cycle) of ZIm^{GAD2} neurons during the time-period that the mouse nose is in the nose poke port. The infrared sensor in the other nose poke port did not trigger any photo stimulation. The test was 1 hour. Number of returns to each port was detected by the sensors and sent to MATLAB for counting number of returns to the nose poke ports.

Familiar open field test

Mice with expression of stGtACR2 or tdTomato (control) in ZIm^{GAD2} were habituated to the experimenter and the open field box (35 cm × 35 cm × 35 cm) every day for three weeks. For the test in the open field box, mice were receiving 0 Hz optogenetic light through optic fibers (N.A.: 0.39) for the entire time (5 minutes). Mice tracks were analyzed using Bonsai software (https://open-ephys.org/bonsai).

Multi-fluorescence mRNA in-situ hybridization (RNAscope)

In-situ hybridization was performed using RNAscope Technology. We used C57BL/6 mice for these experiments. After induction of deep-anesthesia by isoflurane (5%), brains were extracted and immediately fresh-frozen in optimal cutting temperature (OCT). Using a cryostat, brains were sliced into 10 µm sections, mounted on glass slides, and stored at -80 °C. Multi-fluorescence mRNA situ hybridization was performed using ACDBio RNAscope multiplex fluorescence assay (https://acdbio.com/). The RNAscope protocol was carried out as indicated in the user manual of the ACDBio RNAscope. The brain sections of ZIm were post-fixed with 4% chilled paraformaldehyde (PFA in PBS) for 15 min and then dehydrated through four dehydration steps in 50%, 75%, 100%, and 100% ethanol (5-min each), respectively, at room temperature (RT). After air drying for 5 min at RT, Protease IV was applied to the slices for 35 min at RT. Then, they were 3 times washed out by rinsing in phosphate-buffered saline (PBS). TAC1-C1 (Cat No.

410351) and VGAT-C2 (Cat No. 319191-C2) (for **Fig. 6, A and B**) or TAC1-C1, PV-C2 (Cat No. 421931-C2) and SST-C3 (Cat No. 404631-C3) (for **Fig. 6, C and D**) were pipetted onto each slice. Probe hybridization took place in an oven set to 40 °C for 2 hr, and then, slices were rinsed in 1 × wash buffer. After incubation at 40 °C in four-step amplifications (Amp1 for 30 min, Amp2 for 15 min, Amp3 for 30 min, and Amp4 for 15 min), slices were mounted with DAPI (4',6-diamidino-2-phenylindole) vector shield. Immediately after mounting, the stained slices were imaged by confocal SP8 microscope (Leica) using a 20X objective. For quantification of number of labeled and co-labeled cells we used ImageJ (Fiji) and a custom-written MATLAB program.

Immunohistochemistry

TAC1-Cre×Ai14 mice were perfused with 4% PFA in PBS, brains were dissected out and post-fixed for 2 hours. Next, we sliced them into 50 µm coronal sections and incubated the slices for 2 hours in blocking solution (0.1% Triton X-100, 5% NGS in PBS) on a rotary shaker at room temperature. Next, they were incubated with primary antibodies, rabbit anti-parvalbumin (Swant, 1:1000) and rat anti-somatostatin (Millipore, 1:250), in normal goat serum blocking solution overnight at 4 °C. The next day we washed the slices with 3 times with washing solution (0.1% Tween in PBS) (10 minutes each) and incubated the slices in the secondary antibody solution, goat anti-rabbit Alexa 405 (Life Technologies, 1:500) and goat anti-rat Alexa 488 (Life Technologies, 1:700) in blocking solution for 1 hour at room temperature on the rotary shaker. Next, we washed the slices in the washing solution 3 times for 10 minutes at room temperature on the rotary shaker. Stained sections were mounted on glass slides with mowiol. The stained slices were imaged by confocal SP5 microscope (Leica) using a 20X objective.

Overall experimental design and analysis

No statistical methods were used to predetermine sample sizes, but our sample sizes were determined based on previous studies (*7*, *11*). The order of the animals in different experimental groups was randomly assigned. The objects were randomly assigned to be familiar or novel in the FADC object investigation tests. Experimenters were not blind to the experimental conditions, but the collected data were encoded blindly (using a MATLAB code) and analyzers were blind to the experimental conditions. All data were analyzed using JAABA, MATLAB and Bonsai.

Statistical analysis

Data are represented as mean ± SEM. All the statistical analysis was done using a homemade MATLAB toolbox, InVivoTools (https://github.com/heimel/InVivoTools). First, normality of the data distribution were checked, using Shapiro-Wilk normality test. In order to assess group statistical significance, in case the data were normally distributed we used parametric tests (i.e. t-test and paired t-test for non-paired and paired comparisons, respectively) and otherwise non-parametric tests (i.e. Mann-Whitney U test and Wilcoxon signed rank test for non-paired and paired comparisons, respectively), followed by a Bonferroni p-value correction for multi group comparisons. Where we used correlation analysis, the significance level is 0.05. To compare the photometry signals in Fig. 3-5 we used two-way ANOVA followed by a Tukey-Kramer post hoc test.

Individual data points are shown in the figures. All the statistics used in figures and supplementary figures are shown in tables of statistics (**Table S1 and S2**).

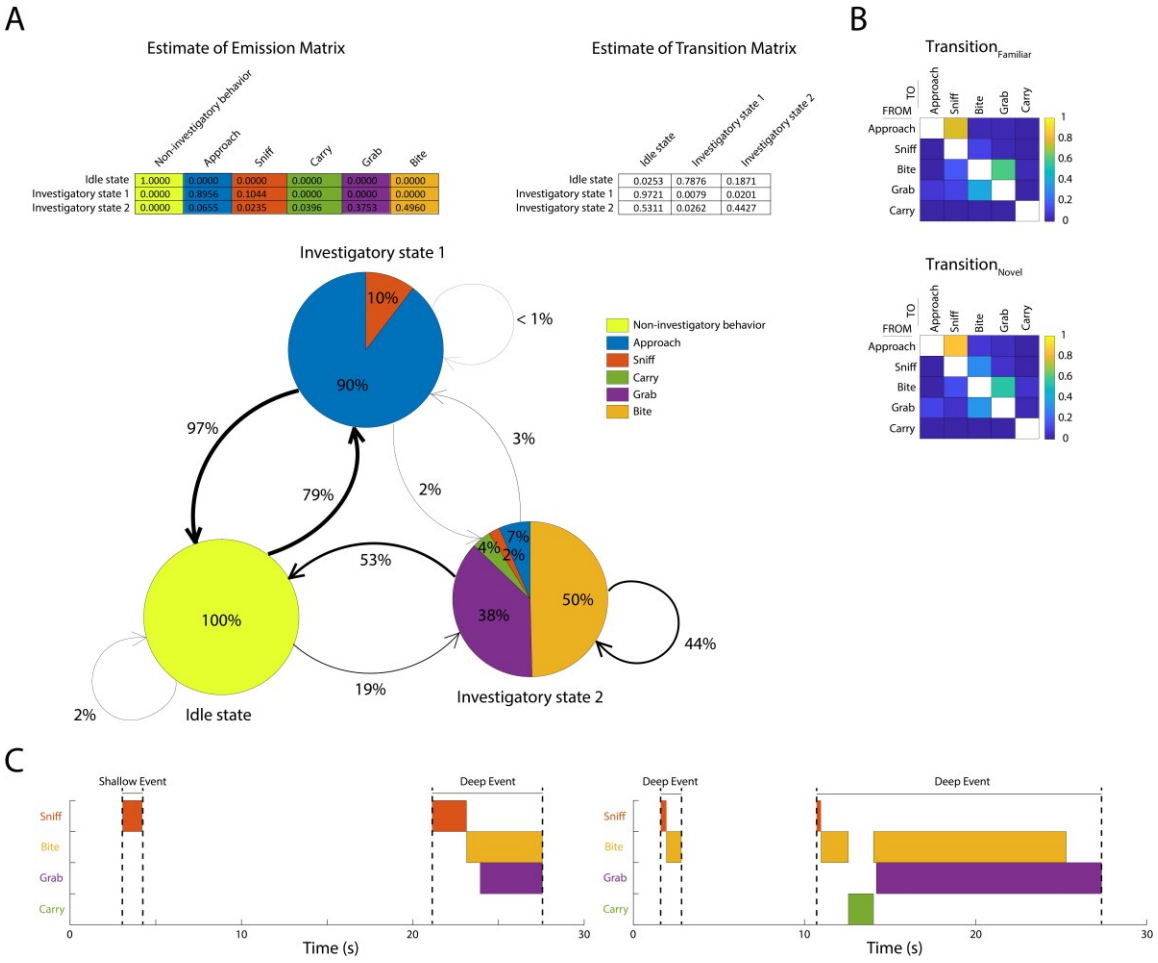

Fig S1: (**A**) Representation of Hidden Markov Model (HMM) of the behavior of C57BL/6 mice in the object interaction test (n = 37 tests from 8 mice). Using labeled behaviors of approach, sniff, bite, grab and idle (no investigative action) of the mice, HMM estimated the emission matrix of three states (idle, investigatory state 1 and investigatory state 2) and the matrix of probability of transitions between the states. The two states of investigatory behavior estimated by the HMM are: investigatory state 1: approach and sniff without any other investigatory action and investigatory state 2: approach and sniff with other investigatory actions (with the highest probability of biting). (**B**) Representation of the transition matrices of actions taken by C57BL/6 mice in interaction with familiar objects (top) and novel objects (bottom) by the C57BL/6 mice (n = 37 tests from 8 mice). (**C**) Examples of shallow and deep object investigation events.

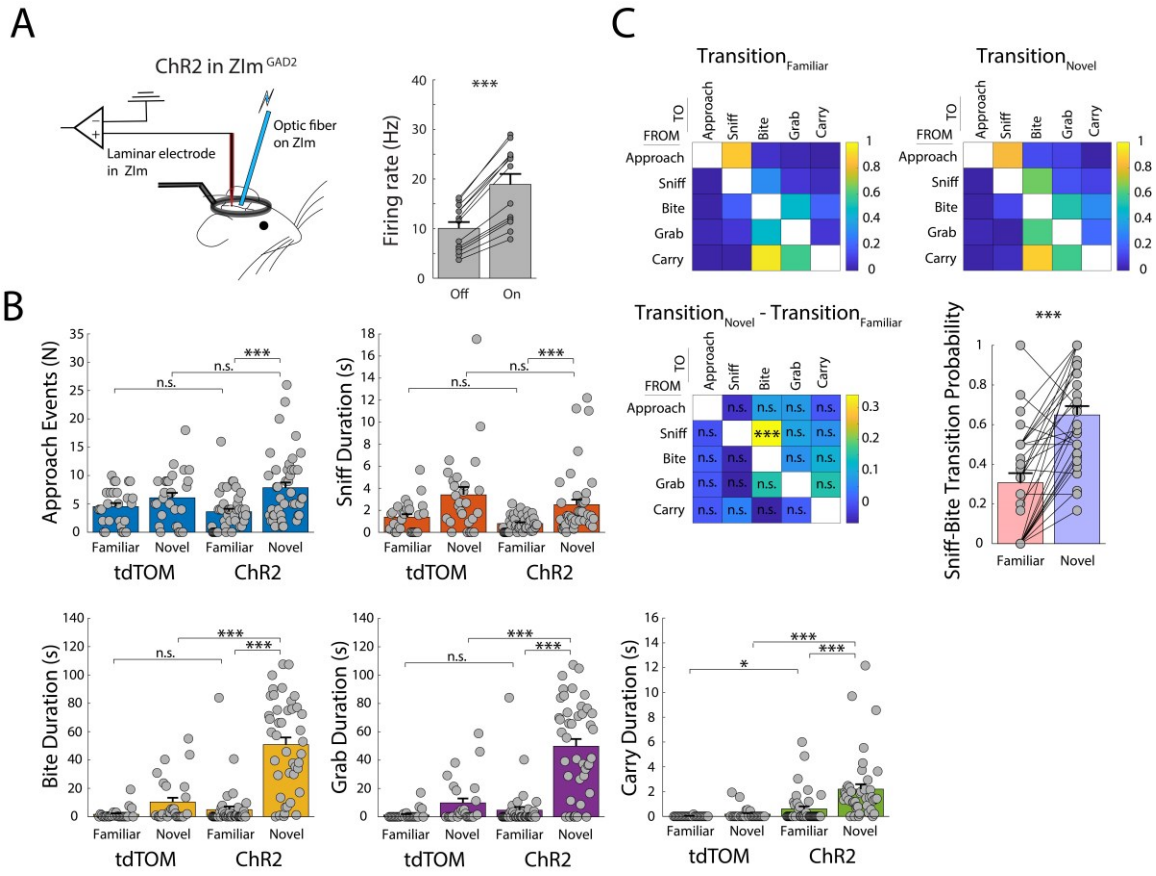

Fig S2: (**A**) Left: Schematic of in-vivo extracellular recording from ZIm while photo stimulating the ZIm^{GAD2} neurons. Right: Bar graph of firing rate (Hz) of the ZIm units (13 units) when the photo stimulation light is off and on. (**B**) Bar graphs show number of approaches and duration of actions (sniff, bite, grab and carry) taken by control mice with tdTomato (n = 27 tests from 4 mice) and mice with ChR2-mCherry (n = 42 tests from 7 mice) in 2-min FADC tests with familiar and novel objects. (**C**) Representation of the transition matrices of actions in familiar object (top left) and novel object (top right) interactions taken by the photo stimulated ChR2-mCherry mice used in (A). Bottom left shows the difference between the familiar and novel transition matrices. Bar graph shows probability of sniff to bite transition in interaction with familiar and novel objects. n.s.: not significant, *: <0.05, **: <0.01 and ***: <0.001.

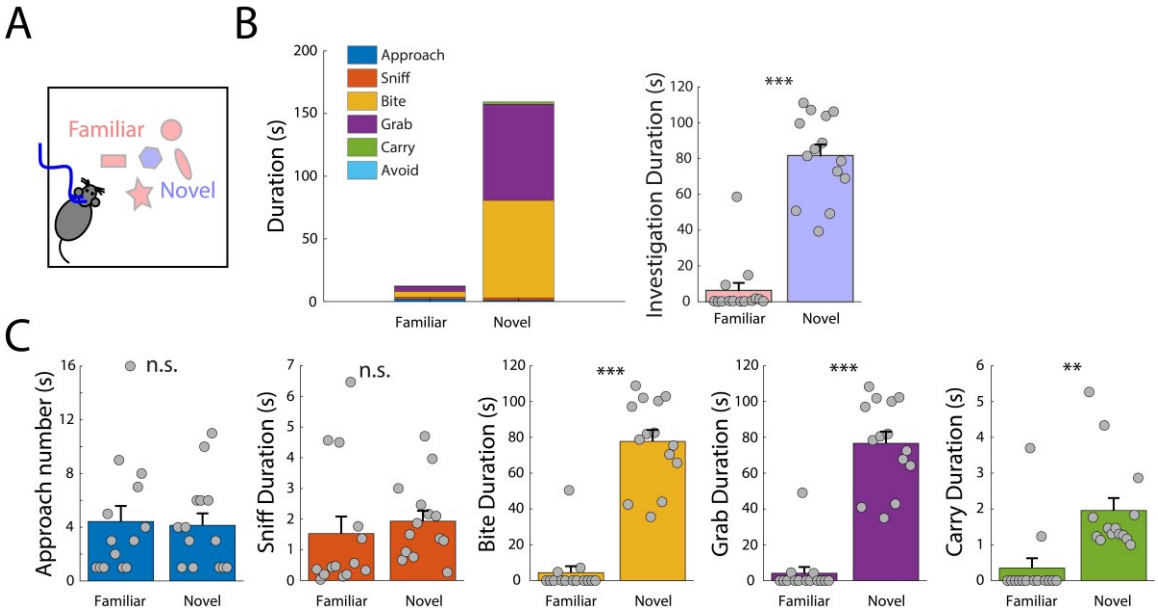

Fig S3: (**A**) Schematics of an FADC with four familiar objects and one novel object for ChR2-mCherry mice. (**B**) The stacked bar graph (left) and the bar graph (right) show duration of the actions and duration of investigation with photoactivation of ZIm^{GAD2} neurons in a 2-min test (n = 14 tests from 5 mice), respectively. (**C**) Bar graphs show number of approaches and duration of actions (sniff, bite, grab and carry) in interaction with the familiar and novel objects taken by the ChR2-mCherry mice in the test. n.s.: not significant, *: <0.05, **: <0.01 and ***: <0.001.

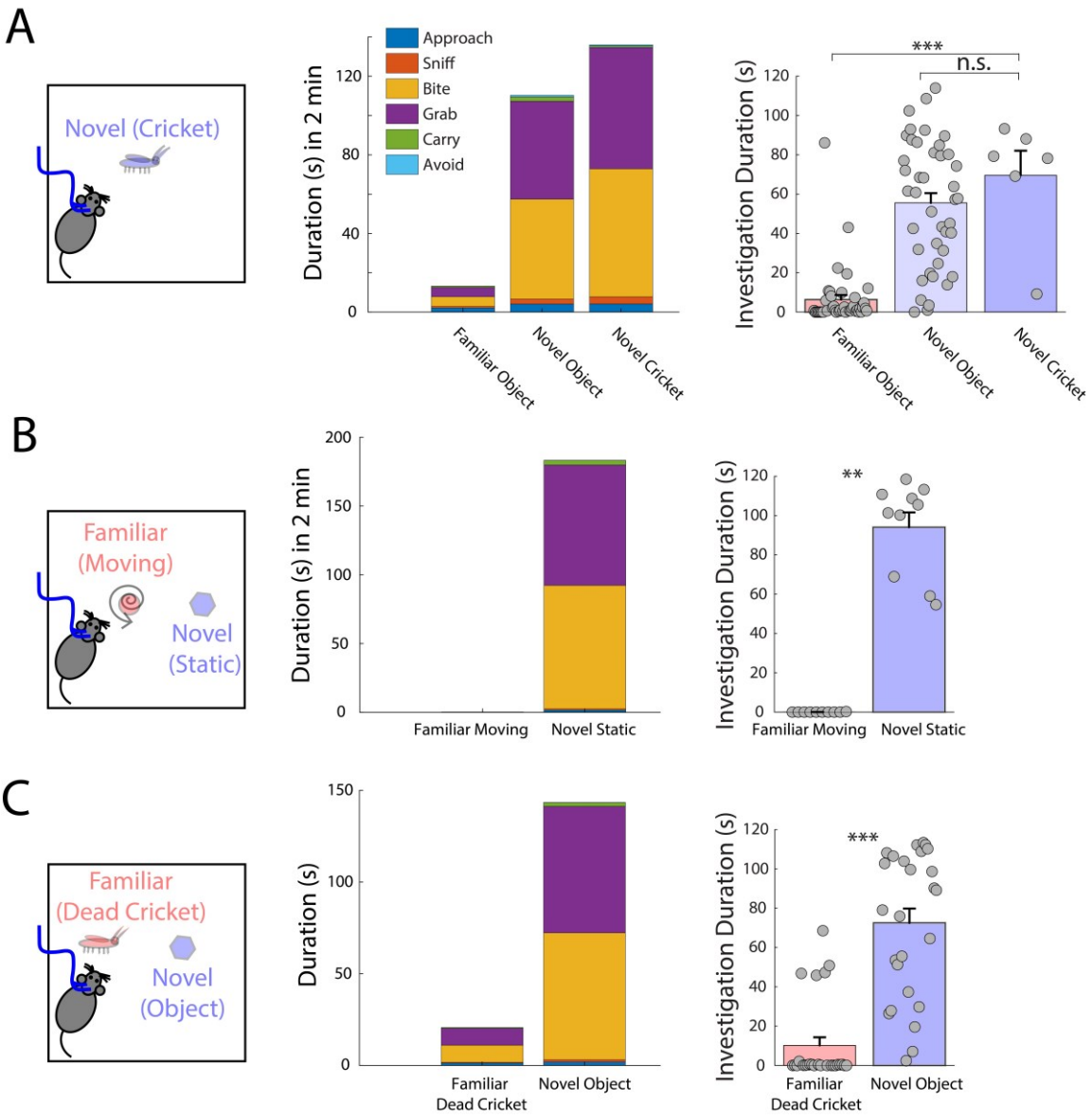

Fig S4: (**A**) Schematics of an interaction test (single choice) with a novel cricket (not introduced in the last 10 min) in ChR2-mCherry mice. The stacked bar graph and the bar graph show duration of the actions and duration of investigation with photoactivation of ZIm^{GAD2} neurons in a 2-min FADC test with familiar and novel objects (n = 42 tests from 7 mice) and in a separate 2-min single novel cricket test (n = 6 tests from 6 mice). (**B**) Schematics of a FADC with a familiar moving object and a novel static object. The stacked bar graph and the bar graph show duration of the actions and duration of investigation with photoactivation of ZIm^{GAD2} neurons in a 2-min test (n = 10 tests from 6 mice). (**C**) Schematics of an FADC with a familiar dead cricket and a novel object. The stacked bar graph and the bar graph show duration of the actions and duration of investigation with photoactivation of ZIm^{GAD2} neurons in a 2-min test (n = 26 tests from 7 mice). n.s.: not significant, **: <0.01 and ***: <0.001.

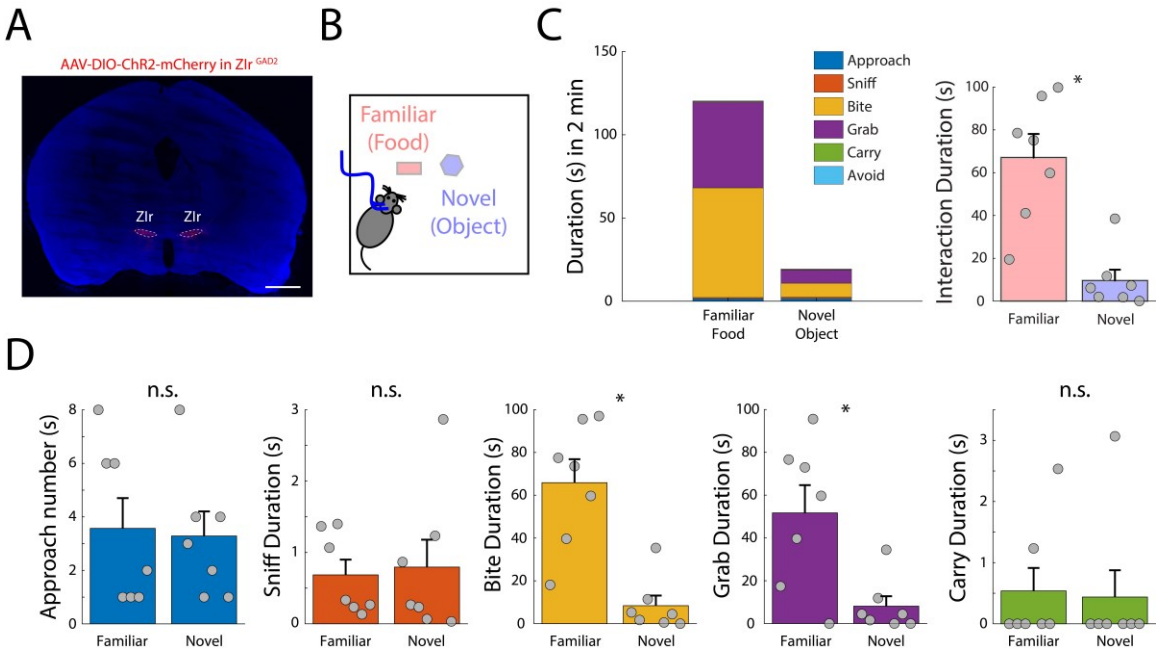

Fig S5: (**A**) Example of expression of AAV-ChR2-mCherry in ZIr of a GAD2-Cre mouse. (**B**) Schematics of a FADC with a familiar food and a novel object. (**C**) The stacked bar graph (left) and the bar graph (right) show duration of the actions and duration of interaction with photoactivation of ZIr^{GAD2} neurons in a 2-min test (n = 7 tests from 3 mice). (**D**) Bar graphs show number of approaches and duration of actions (sniff, bite, grab and carry) in interaction with the familiar food and novel object taken by the ChR2-mCherry mice in the test. n.s.: not significant and *: <0.05.

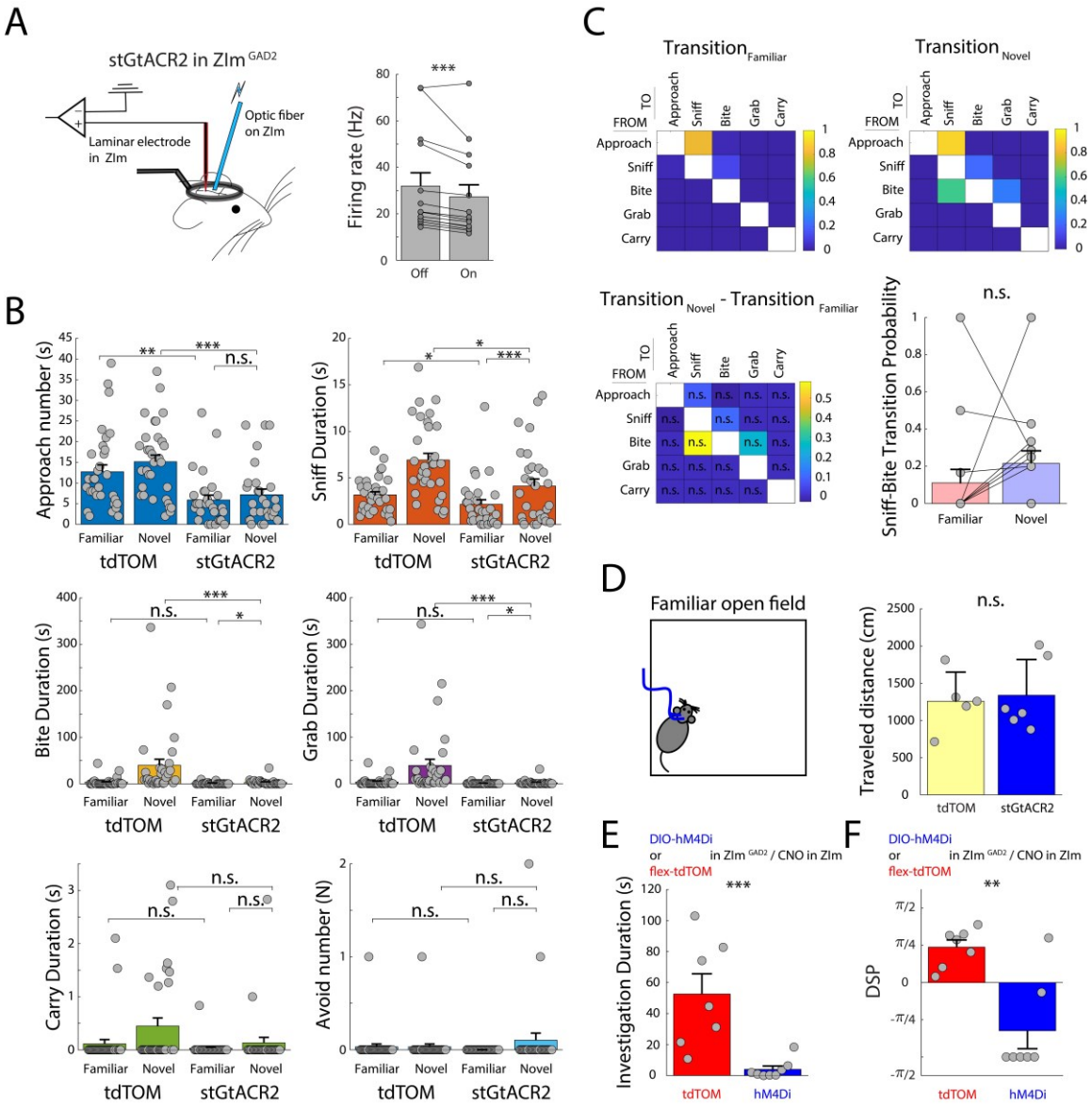

Fig S6: (**A**) Left: Schematic of in-vivo extracellular recording from ZIm while photo inhibiting the ZIm^{GAD2} neurons. Right: Bar graph of firing rate (Hz) of the ZIm units (14 units) when the photo inhibition light is off and on. (**B**) Bar graphs show number of approaches and duration of actions (sniff, bite, grab and carry) taken by control mice with tdTomato (n = 32 tests from 5 mice) and mice with stGtACR2-FusionRed expression in ZIm^{GAD2} (n = 29 tests from 7 mice) in 10-min FADC tests with familiar and novel objects. (**C**) Representation of the transition matrices of actions in familiar object (top left) and novel object (top right) interactions taken by the photo inhibited stGtACR2-FusionRed mice used in (A). Bottom left shows the difference between the familiar and novel transition matrices. Bar graph shows probability of sniff to bite transition in interaction with familiar and novel objects. (**D**) Left: Schematic of a familiar open field test (5 min) of a mouse while photo inhibiting the ZIm^{GAD2} neurons. Right: Bar graph of the travelled distance in the control GAD2-tdTomato mice (n = 5 mice) and GAD2-stGtACR2 mice (n = 6 mice). (**E**) Bar graph of object investigation duration in 10-min

FADC tests of mice expressing tdTOM (n = 7 tests from 3 mice (2 males)) and hM4Di (n = 8 tests from 3 mice (2 males)) in ZIm^{GAD2} after injecting CNO locally in ZIm. (**F**) Bar graph shows DSP of mice in (E). n.s.: not significant, *: <0.05, **: <0.01 and ***: <0.001.

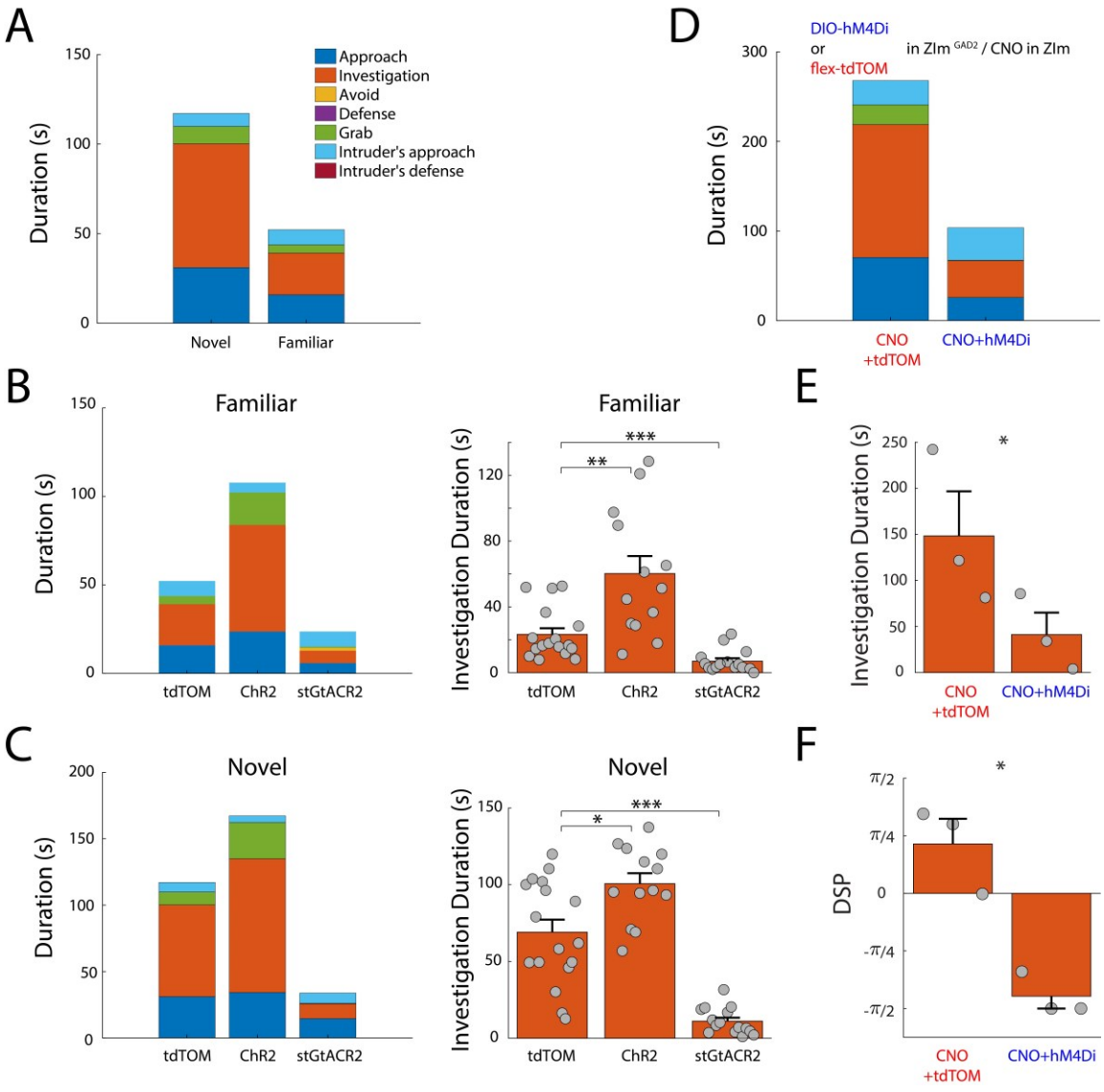

Fig S7: (**A**) The stacked bar graph shows duration of actions (approach, investigation, avoid, defense, grab, intruder's approach and intruder's defense) in the social interaction test (averaged over all tests) in control tdTomato mice (n = 17 tests from 8 mice). (**B**) The stacked bar graph (left) shows duration for actions and the bar graph (right) shows investigation duration of tdTom (n = 17 tests from 8 mice), ChR2 (n = 13 tests from 5 mice) and stGtACR2 (n = 15 tests from 6 mice) mice in the familiar period of the social interaction test. (**C**) The stacked bar graph (left) shows duration for actions and the bar graph (right) shows investigation duration of tdTomato, ChR2 and stGtACR2 mice in the novel period of the social interaction test. (**D**) Stacked bar graph of duration of actions, in social interaction test, taken by mice expressing tdTomato (n = 3 tests from 3 mice (2 males)) and hM4Di (n = 3 tests from 3 mice (2 males)) in ZIm^{GAD2} after injecting CNO locally in ZIm. (**E**) Bar graph shows investigation duration of mice in (D). (**F**) Bar graph shows DSP of mice in (D). *: <0.05, **: <0.01 and ***: <0.001.

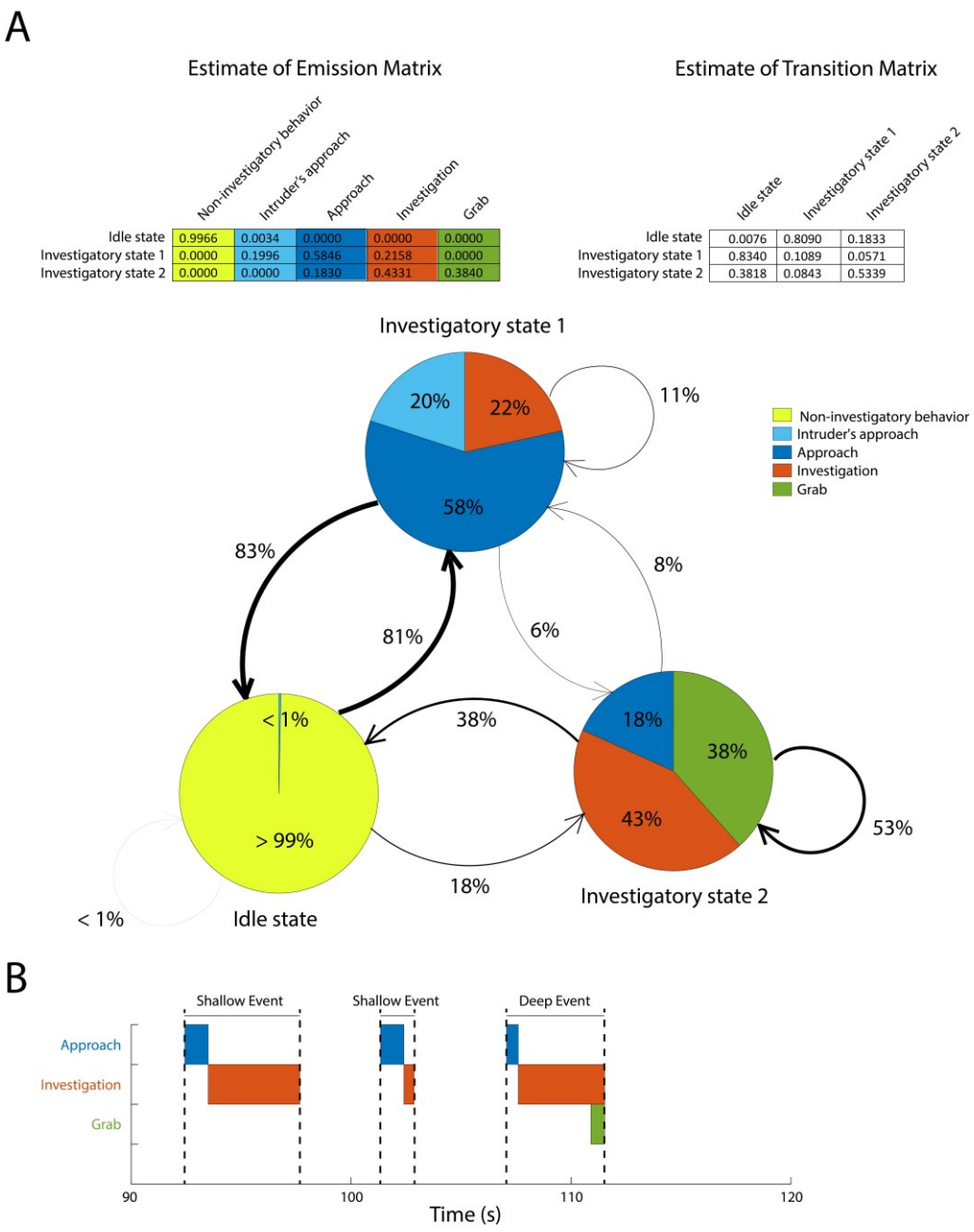

Fig S8: (**A**) Representation of Hidden Markov Model (HMM) of the behavior of control tdTomato mice in the social interaction test (n = 17 tests from 8 mice). Using labeled behaviors of intruder's approach, approach, investigation, grab and idle (no investigative action) of the control tdTomato mice, HMM estimated the emission matrix of three states (idle, investigatory state 1 and investigatory state 2) and the matrix of probability of transitions between the states. The two states of investigatory behavior estimated by the HMM are: investigatory state 1: approach and investigation without grab and investigatory state 2: approach and investigation with grab. (**B**) Examples of shallow and deep social investigation events.

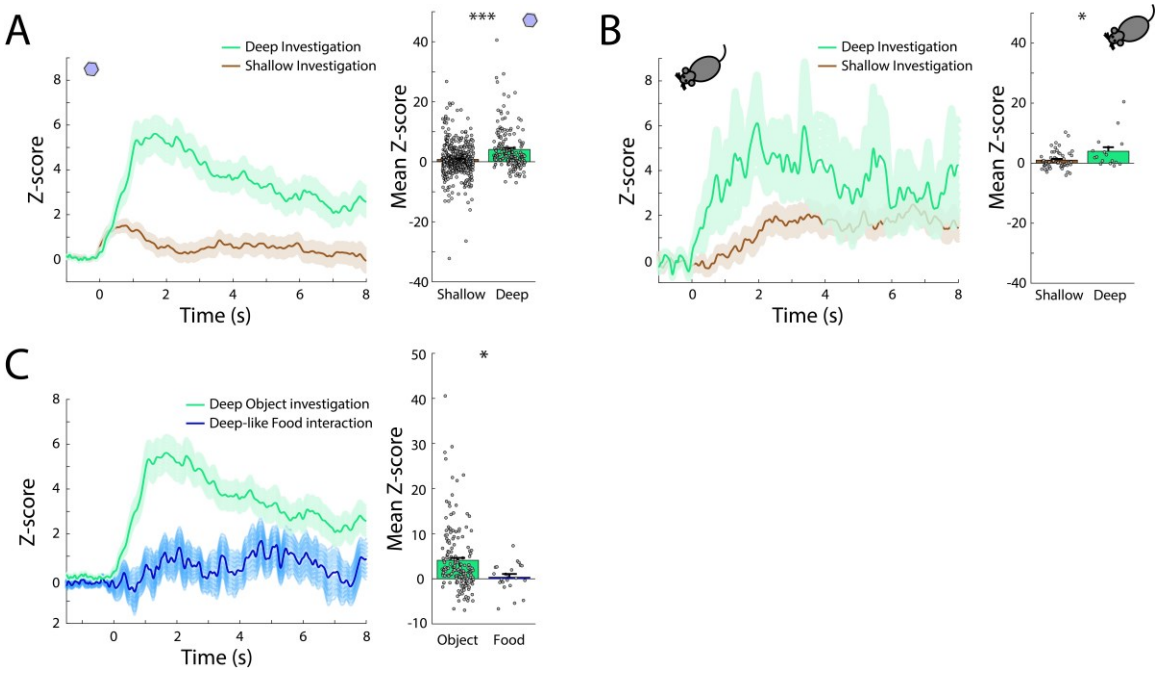

Fig S9: (**A**) Left: photometry signals of ZIm^{GAD2} neurons during Deep (174 tests) and Shallow (451 tests) investigation of objects, averaged over all object investigation events (6 mice). Time 0 s indicates start of the object investigation event, i.e. start of sniffing. Dark and the surrounding light colors represent mean±SEM. Right: Bar graph shows mean Z-score of signals. (**B**) Left: photometry signals of ZIm^{GAD2} neurons during Deep (17 tests) and Shallow (56 tests) social investigation, averaged over all social investigation events (8 mice). Time 0 s indicates start of the social investigation event, i.e. start of approaching the intruder conspecific. Dark and the surrounding light colors represent mean±SEM. Right: Bar graph shows mean Z-score of signals. (**C**) Left: photometry signals of ZIm^{GAD2} neurons during Deep object investigation events (174 tests) and Deep-like food interaction events (22 tests), averaged over all events (6 mice). Deep-like food interaction event is the same as event of actions taken during Deep object investigation, but having food pellet instead of the object. Time 0 s indicates start of the object or food interaction event, i.e. start of sniffing. Dark and the surrounding light colors represent mean±SEM. Right: Bar graph shows mean Z-score of signals.

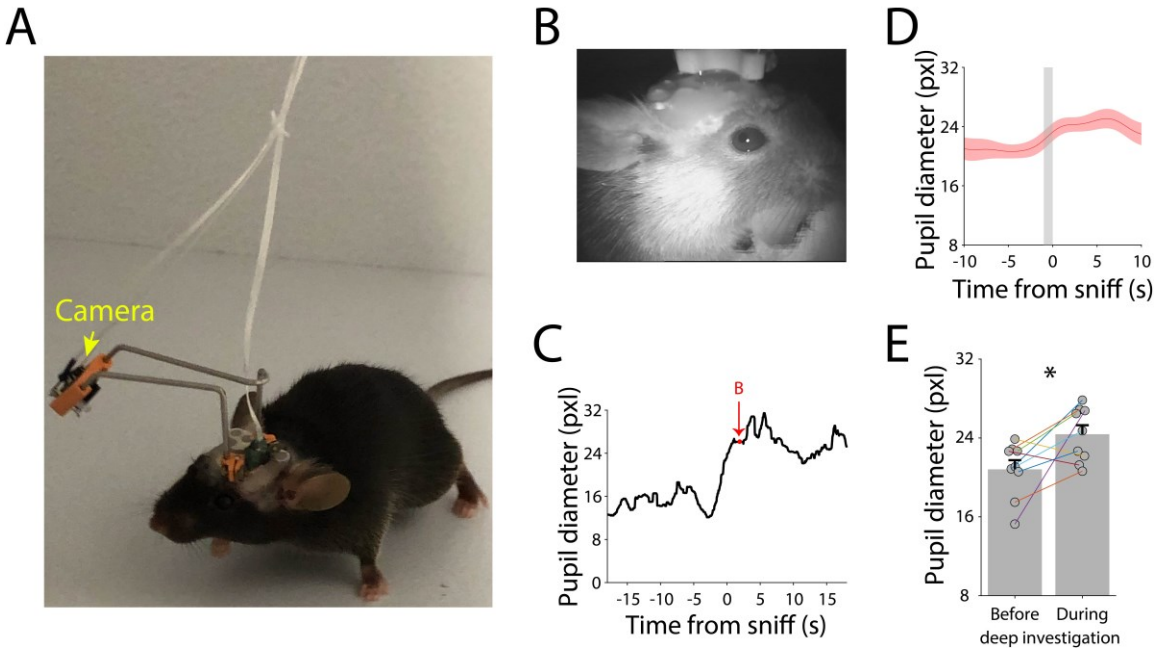

Fig S10: (**A**) Head mounted IR camera in a freely moving mouse (**B**) Example image captured by head mounted IR camera in a freely moving mouse during deep investigation. The investigated object is visible between the paws and the snout. (**C**) Pupil diameter in the 10s preceding the first sniff of the object and the first 10s of the investigation. Red arrow indicates the point at which the image in B was taken. (**D**) Average pupil diameter during the first 10s of deep investigation after the sniff onset (0 s) (9 events in 6 sessions of 2 mice). (**E**) Mean pupil diameter during the 10s directly before the investigation and the first 10s of the investigation in the experiments shown in (D). *: <0.05.

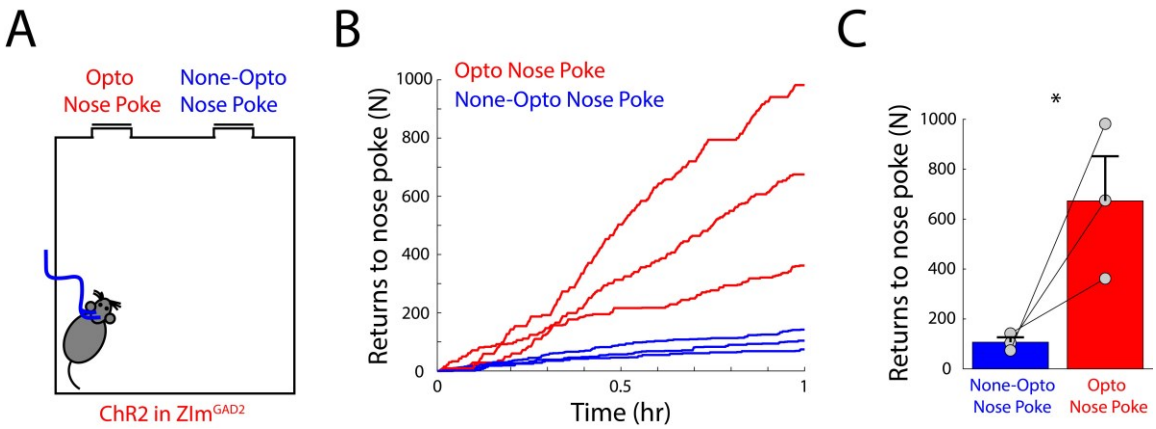

Fig S11: (**A**) Schematic of self-stimulation nose poke test in ZIm^{GAD2} ChR2-expressing mice. An infrared sensor in one nose poke leads to optogenetic activation of ZIm^{GAD2} neurons during the time-period that the mouse nose is in the nose poke hole. The infrared sensor in the other nose poke hole does not trigger any photo stimulation. (**B**) Cumulative histogram of number of returns to the photo-stimulating (red) and none- photo-stimulating (blue) nose pokes (3 mice). (**C**) Bar graph of number of returns to the nose pokes. *: <0.05.

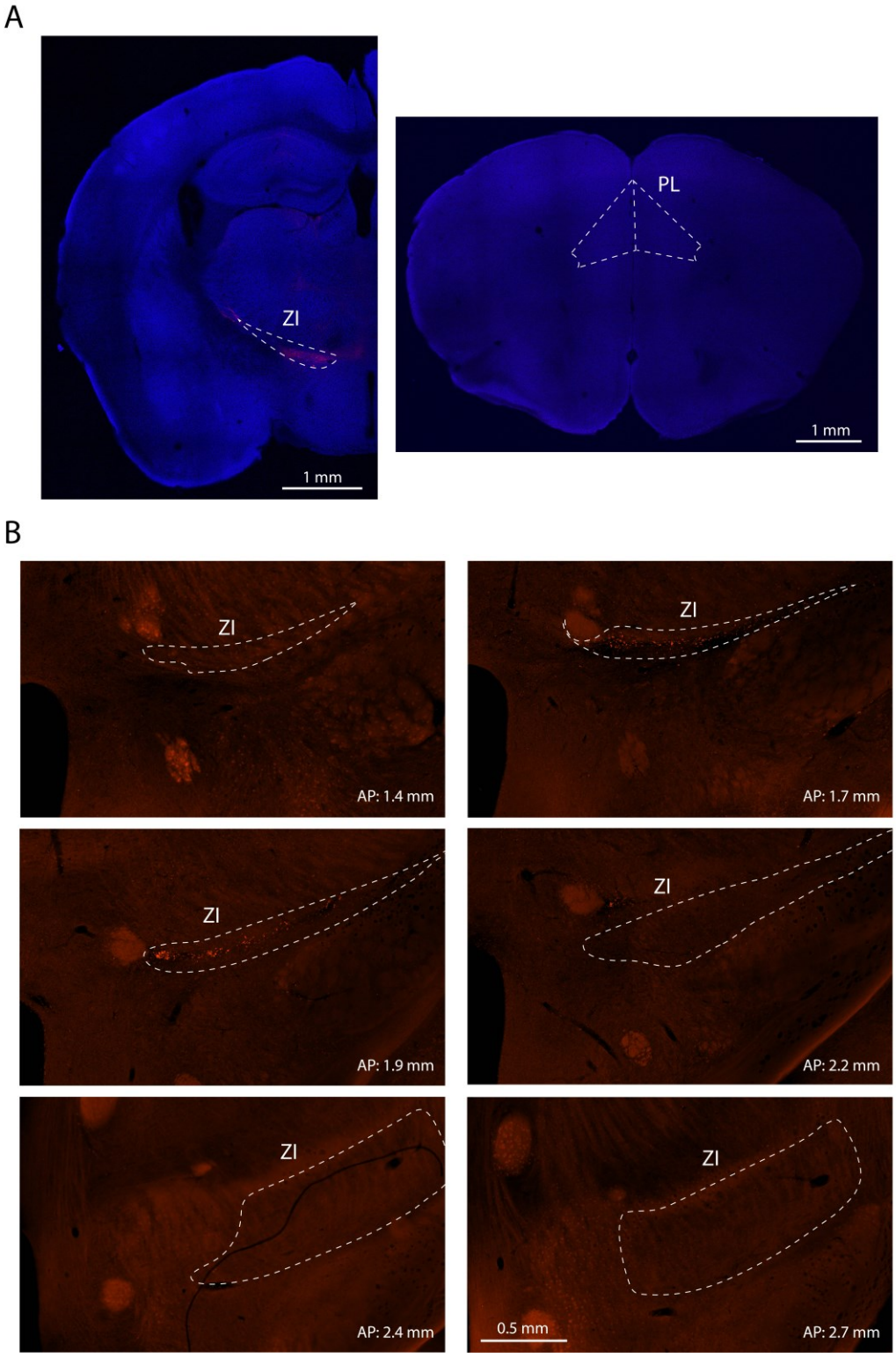

Fig S12: (**A**) Expression of Cre-dependent retroAAV-mCherry in ZIm (left; injection site) of a GAD2-Cre mouse and absence of mCherry expression in the PL neurons (right). (**B**) Expression of EYFP (shown in red) in PL→ZI axons in different coronal sections of ZI a C57BL/6 mouse with AAV-CAMKII-ChR2-EYFP injection in PL. AP indicates the distance from Bregma in anterior-posterior axis.

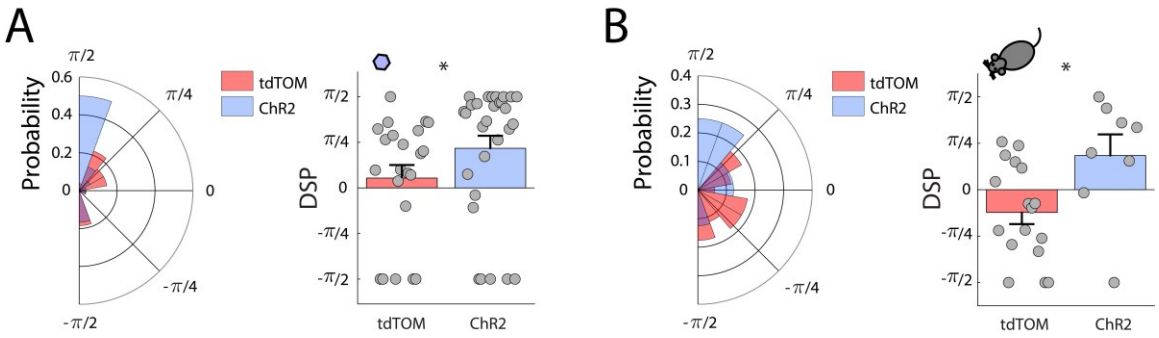

Fig S13: (**A**) Probability histogram and bar graph of DSP index of control mice with tdTomato (n = 27 tests from 4 mice) and mice with photoactivation of ZIm^{GAD2} → PAG projection (n = 30 tests from 5 mice) in interaction with novel objects. (**B**) Probability histogram and bar graph of DSP index of control mice with tdTomato (n = 17 tests from 8 mice) and mice with photoactivation of ZIm^{GAD2} → PAG projection (n = 8 tests from 5 mice) in the novel period of the social interaction. *: <0.05.

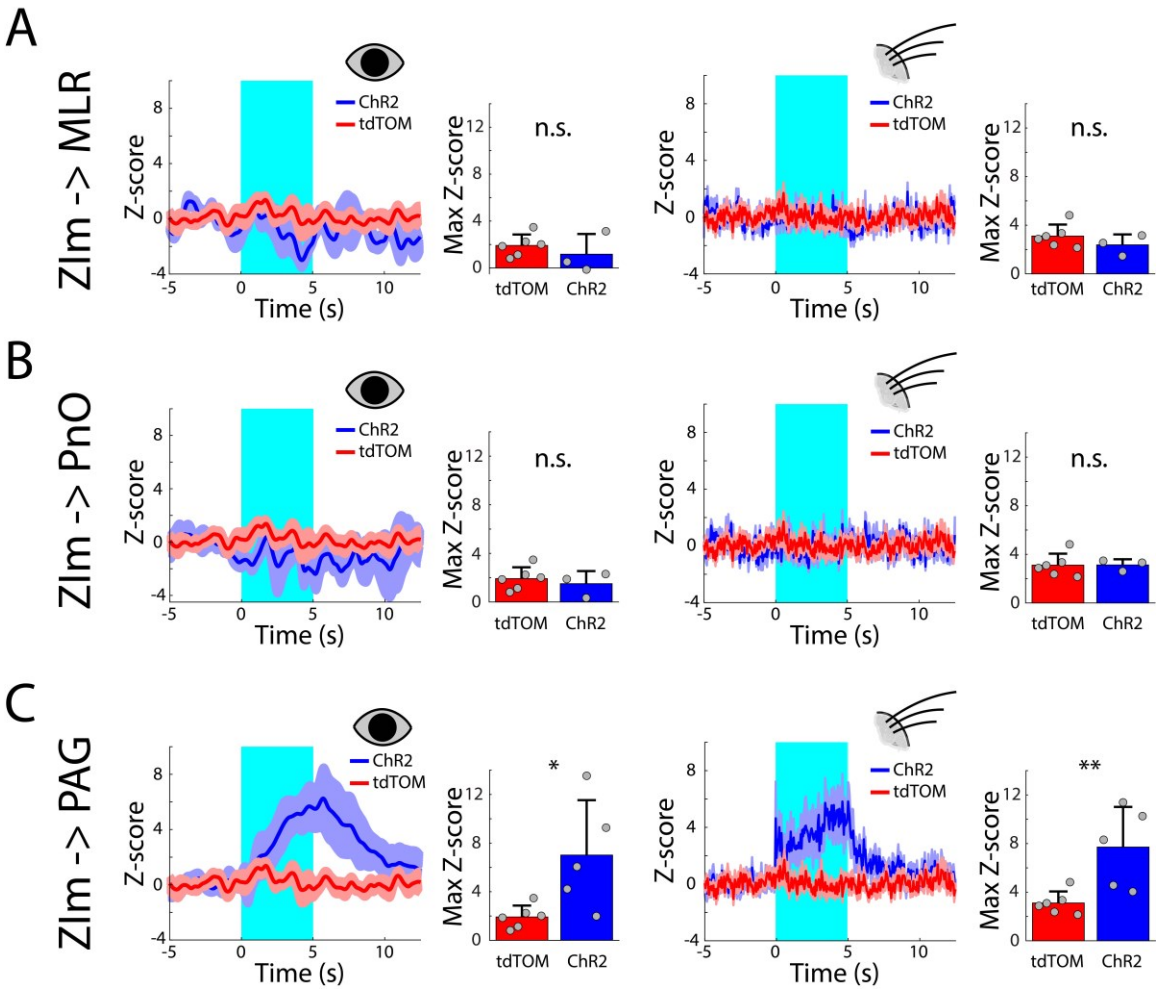

Fig S14: (**A**) Z-score and maximum Z-score of pupil size (the right two) and whisker activity (the left two) of tdTom (red; n = 6 mice) and ChR2 (blue; n = 3 mice) mice. ZIm^{GAD2} → MLR axons are photo stimulated from 0 to 5 s. (**B**) Z-score and maximum Z-score of pupil size (the right two) and whisker activity (the left two) of tdTom (red; n = 6 mice) and ChR2 (blue; n = 3 mice) mice. ZIm^{GAD2} → PnO axons are photo stimulated from 0 to 5 s. (**C**) Z-score and maximum Z-score of pupil size (the right two) and whisker activity (the left two) of tdTom (red; n = 6 mice) and ChR2 (blue; n = 5 mice) mice. ZIm^{GAD2} → PAG axons are photo stimulated from 0 to 5 s. n.s.: not significant, *: <0.05 and **: <0.01.

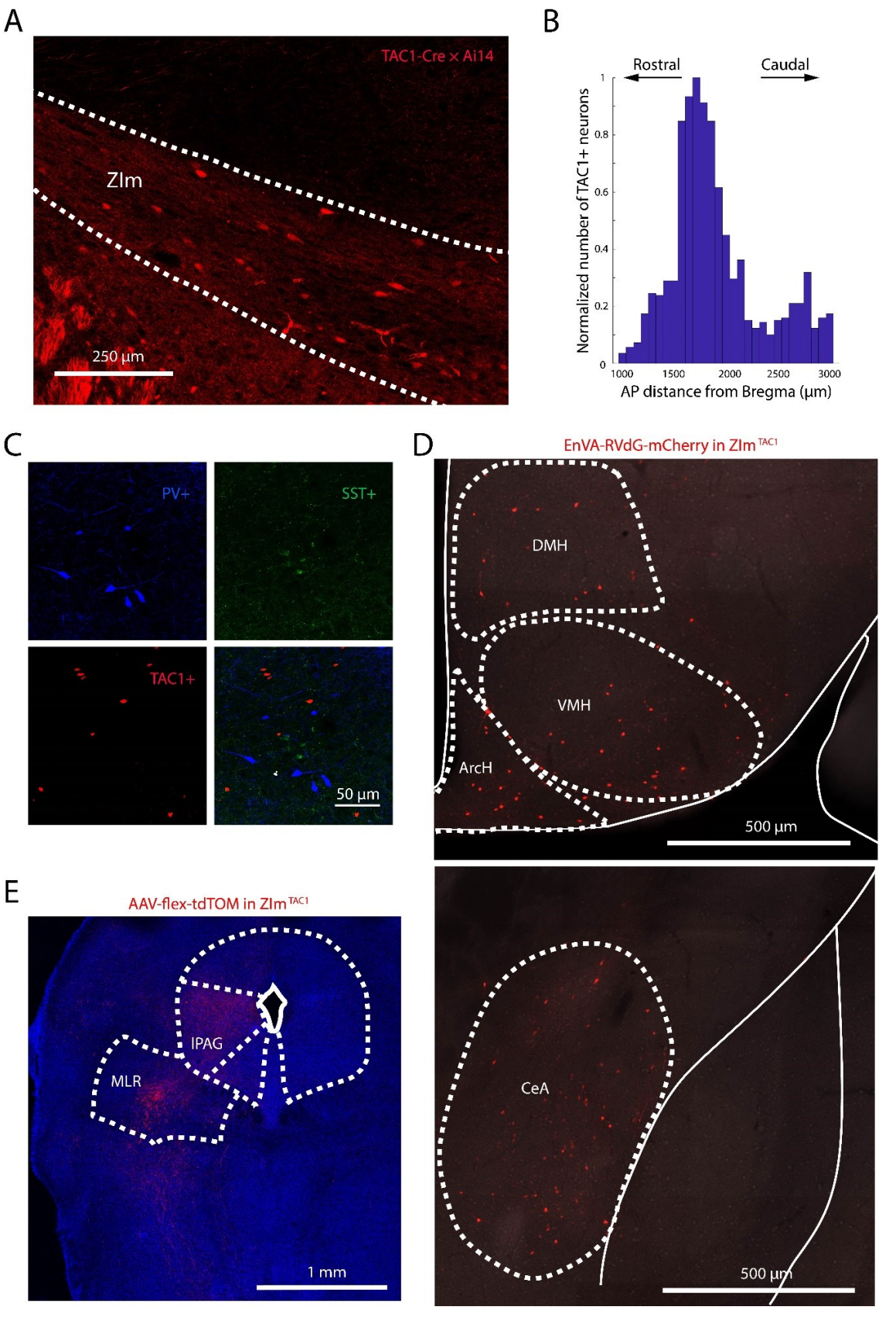
A
TAC1-Cre × Ai14
ZIm
250 µm
B
Rostral
Caudal
Normalized number of TAC1+ neurons
0
0.2
0.4
0.6
0.8
1
1000
1500
2000
2500
3000
AP distance from Bregma (µm)
C
PV+
SST+
TAC1+
50 µm
D
EnVA-RVdG-mCherry in ZIm TAC1
DMH
VMH
ArcH
500 µm
E
AAV-flex-tdTOM in ZIm TAC1
IPAG
MLR
1 mm
CeA
500 µm

Fig S15: (**A**) Expression of tdTomato in ZIm neurons in a TAC1-Cre crossed with tdTomato reporter mouse line (Ai14). (**B**) Number of TAC1+ neurons in ZI (counted from 75-µm slices of two TAC1-Cre × Ai14 mice) over Anterior-Posterior (AP) axis normalized by the slice with the maximum number of ZI^{TAC1} neurons. (**C**) Immunohistochemistry staining of PV and SST (using anti-PV and anti-SST antibodies) in a TAC1-Cre × Ai14 mouse, showing no overlap between PV+, SST+ and TAC1+ neurons. (**D**) Rabies monosynaptic retrograde tracing experiment in a TAC1-Cre mouse (shown in **Fig. 6K**) shows the expression of RVdG in other brain regions than the PL. Top: Expression of RVdG in Dorso-Medial Hypothalamus (DMH), Ventro-Medial Hypothalamus (VMH), Arcuate nucleus of Hypothalamus (ArcH). Bottom: Expression of RVdG in Central Amygdala (CeA). (**E**) ZIm^{TAC1} axons visualized in other brain regions, lPAG and MLR (using an anterograde AAV-flex-tdTOM injection in ZIm^{TAC1}).

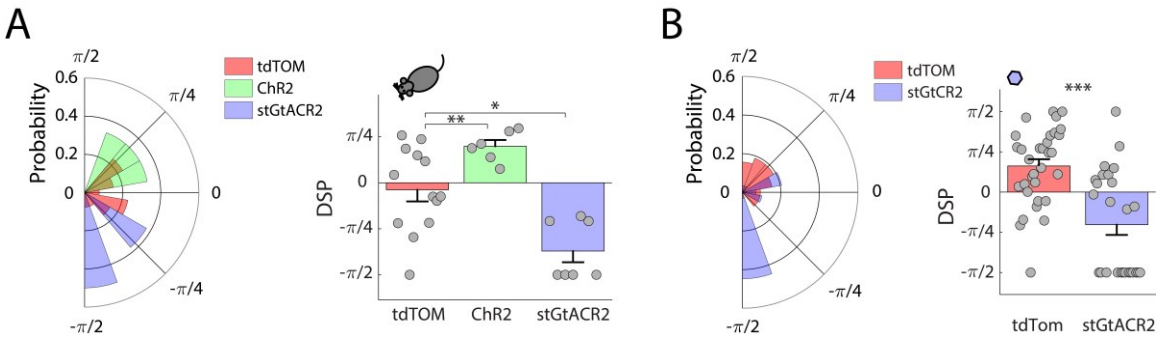

Fig S16: (A) Probability histogram and bar graph of DSP index of control tdTomato mice (n = 13 tests from 4 mice) and mice with expression of ChR2 (n = 6 tests from 5 mice) and stGtACR2 (n = 8 tests from 5 mice; in one test the mouse did not investigate) in ZIm^{TAC1} in social investigation test. (B) Bar graph represents duration of novel object investigation in control tdTomato mice (n = 25 tests from 3 mice) and mice with stGtACR2 expression in ZIm^{TAC1} (n = 9 tests from 3 mice) during 10-min object investigation test. *: <0.05 and **: <0.01.

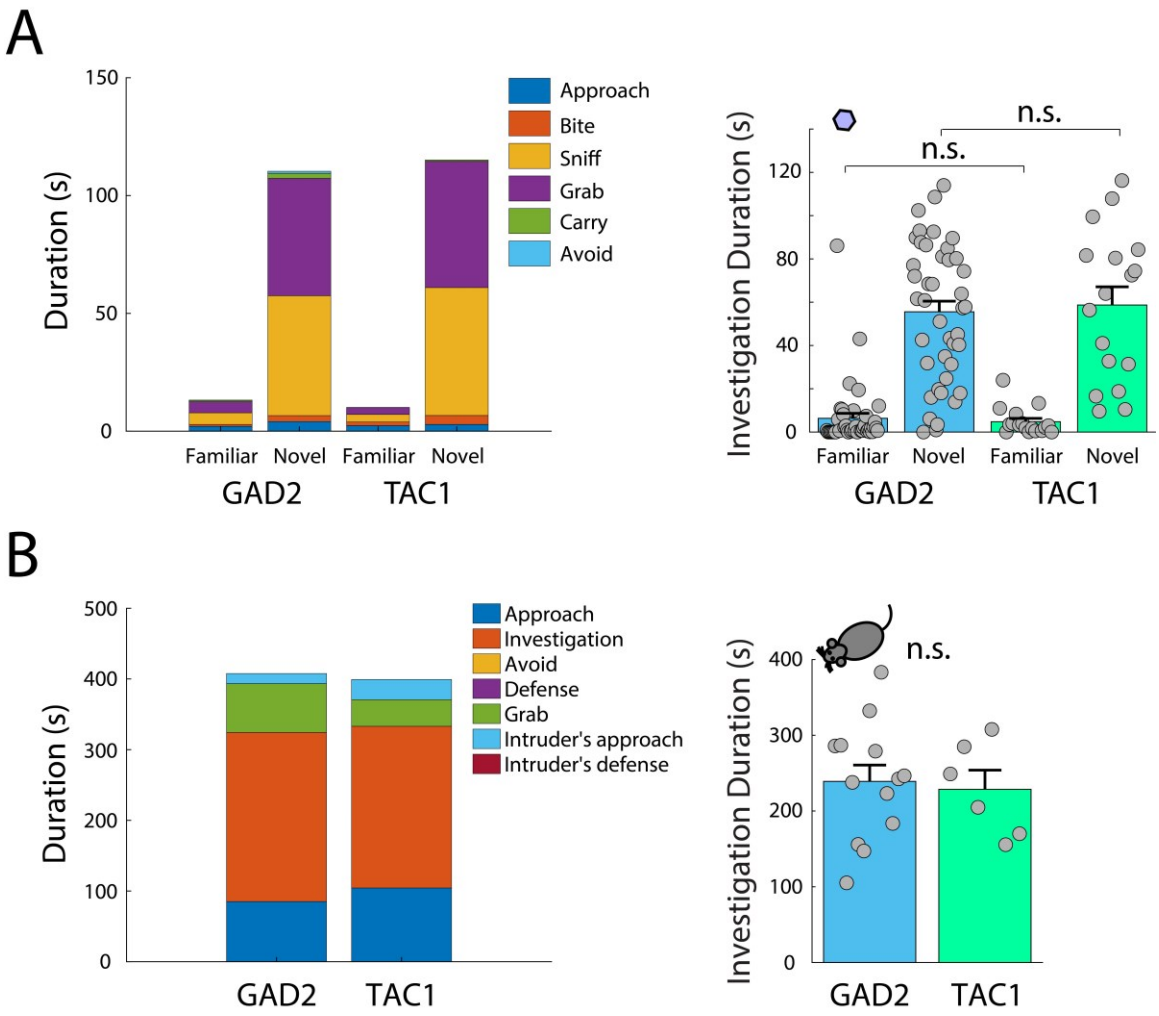

Fig S17: (**A**) Stacked bar graph shows average duration of actions taken by mice with ChR2-mCherry in ZIm^{GAD2} (n = 42 tests from 7 mice) and in ZIm^{TAC1} (n = 17 tests from 5 mice) in 2-min FADC tests with familiar and novel objects. Bar graphs represent duration of the novel object investigation. (**B**) Stacked bar graph shows average duration of actions taken by mice with ChR2-mCherry in ZIm^{GAD2} (n = 13 tests from 5 mice) and in ZIm^{TAC1} (n = 6 tests from 5 mice) in social investigation test. Bar graphs represent duration of the social investigation. n.s.: not significant.

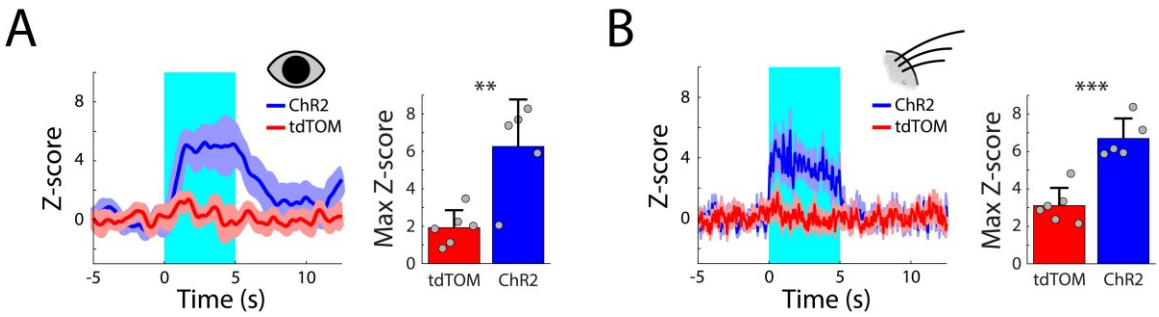

Fig S18: Z-score and maximum Z-score of (**A**) pupil size and (**B**) whisker activity of tdTom (red; n = 6 mice) and ChR2 (blue; n = 5 mice) TAC1-Cre mice. ZIm^{TAC1} neurons are photo stimulated from 0 to 5 s. **: <0.01 and ***: <0.001.

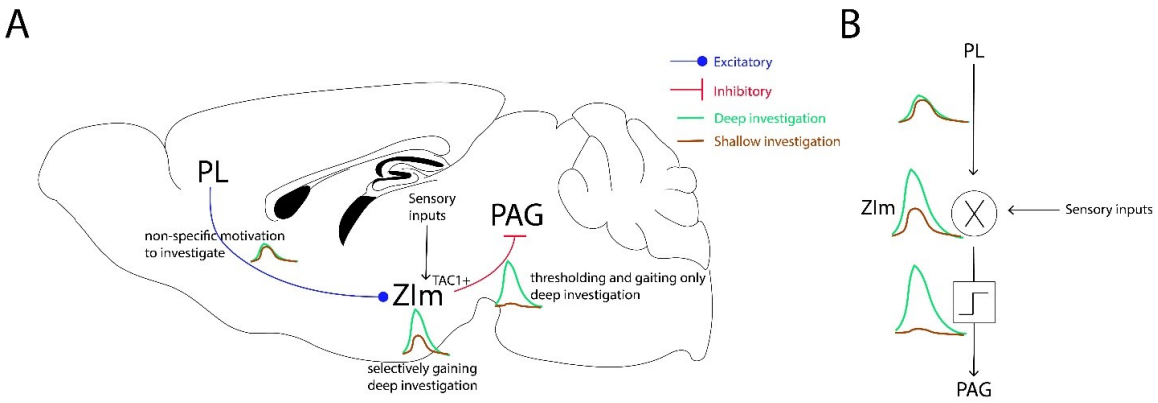

Fig S19: (**A**) Schematic of a hypothetical model for investigation based on our findings. PL excitatory input into ZIm conveys non-specific motivation and arousal level to investigate. ZIm^{GAD2} and more specifically ZIm^{TAC1} neurons using extra information (e.g. sensory inputs from thalamus and midbrain) and processing selectively is gain modulating the deep investigation. A subpopulation of ZIm^{GAD2} neurons (likely to be ZIm^{TAC1} neurons) are setting a threshold on activity of ZIm^{GAD2} neurons and gate only the deep investigation signal into the PAG. (**B**) Schematics of the investigation mechanism in a more abstract way: the initial signal in the PL input to the ZIm is selectively multiplied (possibly using sensory inputs) and after thresholding the deep investigation signal passes into the PAG.

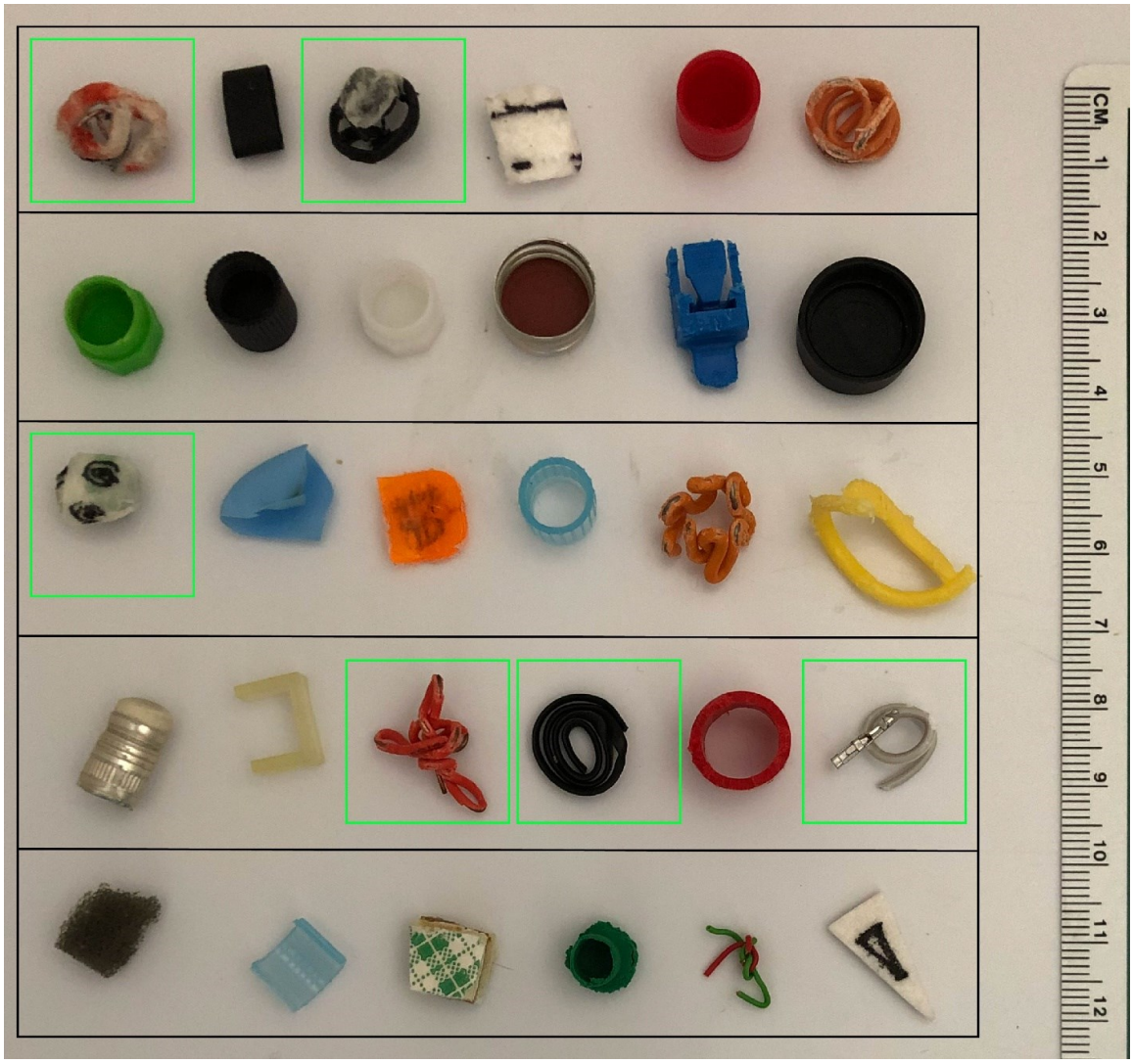

Fig. S20: Thirty of the objects used in the object investigation tests. In case we needed a moving object, the objects shown in the green squares could move using a magnet under the experimental box.

Table S1. Table of statistics of main figures

Figure panel	Mean ± s.e.m.	Comparison	Test	Tails or post-hoc test	Test-statistic	P-value
Fig. 1A Approach	Familiar: 19.62±1.95, Novel: 26.47±2.53	Familiar vs. Novel	Wilcoxon signed rank test	Two-tailed	W = 65.5	P = 0.0011
Fig. 1A Sniff	Familiar: 4.30±0.46, Novel: 9.23±0.94	Familiar vs. Novel	Wilcoxon signed rank test	Two-tailed	W = 19	P = 4.6×10^{-6}
Fig. 1A Bite	Familiar: 14.41±6.48, Novel: 50.10±15.43	Familiar vs. Novel	Wilcoxon signed rank test	Two-tailed	W = 50	P = 0.0003
Fig. 1A Grab	Familiar: 10.90±4.81, Novel: 44.54±14.84	Familiar vs. Novel	Wilcoxon signed rank test	Two-tailed	W = 45	P = 0.0005
Fig. 1A Carry	Familiar: 0.13±0.10, Novel: 0.67±0.22	Familiar vs. Novel	Wilcoxon signed rank test	Two-tailed	W = 13	P = 0.0215
Fig. 1B	Familiar: 0.09±0.02, Novel: 0.30±0.03	Familiar vs. Novel	Wilcoxon signed rank test	Two-tailed	W = 26	P^{*} = 6.8×10^{-5}
Fig. 1C DSP	Familiar: -0.45±0.17, Novel: 0.51±0.12	Familiar vs. Novel	Wilcoxon signed rank test	Two-tailed	W = 49	P = 2.2×10^{-5}
Fig. 1E investig. duration	Familiar tdTOM: 3.01±0.96, Novel tdTOM: 13.90±3.42, Familiar ChR2: 6.34±2.30, Novel ChR2: 55.56±4.92	Novel tdTOM vs. Novel ChR2	Mann-Whitney U test	Two-tailed	U = 531.5	P^{*} = 1.1×10^{-6}
		Familiar tdTOM vs. Familiar ChR2	Mann-Whitney U test	Two-tailed	U = 903.5	P^{*} > 0.9999
		Familiar ChR2 vs. Novel ChR2	Wilcoxon signed rank test	Two-tailed	W = 55	P^{*} = 2.1×10^{-6}
Fig. 1F DSP	tdTOM: 0.17±0.22, ChR2: 0.96±0.12	tdTOM vs. ChR2	Mann-Whitney U test	Two-tailed	U = 445.5	P = 0.0002
Fig. 1G investig. duration	Food: 5.28±4.30, Novel: 58.60±7.80	Food vs. Novel	Wilcoxon signed rank test	Two-tailed	W = 8	P = 0.0007
Fig. 1H investig. duration	Cricket: 2.68±1.57, Novel: 71.05±8.21	Cricket vs. Novel	Wilcoxon signed rank test	Two-tailed	W = 0	P = 0.0004
Fig. 1J investig. duration	Familiar tdTOM: 6.95±1.76, Novel tdTOM: 47.41±13.04, Familiar stGtACR2: 3.07±0.80, Novel stGtACR2: 7.17±1.83	Novel tdTOM vs. Novel stGtACR2	T-test	Two-tailed	t[59] = 2.9113	P^{*} = 0.0153
		Familiar tdTOM vs. Familiar	T-test	Two-tailed	t[59] = 1.9379	P^{*} = 0.1723

		stGtACR2				
		Familiar stGtACR2 vs. Novel stGtACR2	Paired t-test	Two-tailed	t[28] = -3.3955	$P^* = 0.0063$
Fig. 1K DSP	tdTOM: 0.51±0.13, stGtACR2: -0.64±0.20	tdTOM vs. stGtACR2	Mann-Whitney U test	Two-tailed	U = 1195	$P = 7.7\times10^{-5}$

*: Bonferroni corrected p-value.

Fig. 2A	Novel: 69.09±8.15, Familiar: 23.30±3.73	Novel vs. Familiar	Wilcoxon signed rank test	Two-tailed	W = 147	P = 0.0008
Fig. 2B AInv transition prob.	Novel: 0.50±0.04, Familiar: 0.51±0.04	Novel vs. Familiar	Wilcoxon signed rank test	Two-tailed	W = 57.5	P = 0.9012
Fig. 2B AInvG transition prob.	Novel: 0.15±0.03, Familiar: 0.08±0.02	Novel vs. Familiar	Wilcoxon signed rank test	Two-tailed	W = 76	P = 0.0327
Fig. 2C DSP	Novel: -0.38±0.19, Familiar: -1.07±0.18	Novel vs. Familiar	Wilcoxon signed rank test	Two-tailed	W = 95	P = 0.0052
Fig. 2D investig. duration	tdTOM: 131.80±14.49, ChR2: 239.16±21.52, stGtACR2: 28.26±4.43	tdTOM vs. ChR2	T-test	Two-tailed	T[28] = -4.2868	$P^* = 0.0003$
		tdTOM vs. stGtACR2	T-test	Two-tailed	T[30] = 6.4678	$P^* = 7.6\times10^{-7}$
Fig. 2E DSP	tdTOM: -0.38±0.19, ChR2: 0.40±0.19, stGtACR2: -1.23±0.13	tdTOM vs. ChR2	T-test	Two-tailed	t[28] = -2.7665	$P^* = 0.0198$
		tdTOM vs. stGtACR2	T-test	Two-tailed	t[30] = 3.5009	$P^* = 0.0030$

*: Bonferroni corrected p-value.

Fig. 3B		Deep vs. Shallow * Time	Repeated measures ANOVA	Tukey-Kramer: Deep vs. Shallow	F(1,399) = 15.033	$P_{interaction} < 10^{-7}$ $P_{post\text{-}hoc} < 10^{-7}$
Fig. 3C Max Z-score	Shallow: 7.42±0.35, Deep: 11.42±0.99	Deep vs. Shallow	Mann-Whitney U test	Two-tailed	U = 168911	P = 0.0004
Fig. 3C Mean Z-score	Shallow: 0.80±0.24, Deep: 4.09±0.49	Deep vs. Shallow	Mann-Whitney U test	Two-tailed	U = 163129	$P < 10^{-7}$
Fig. 3E pupil	tdTOM: 2.33±0.41, ChR2: 27.7±5.8	tdTOM vs. ChR2	Mann-Whitney U test	Two-tailed	U = 21	P = 0.0004
Fig. 3E whisker	tdTOM: 3.32±0.69, ChR2: 10.9±2.2	tdTOM vs. ChR2	Unequal variances t-test	Two-tailed	t[9.5098] = -3.272	P = 0.0090
Fig. 3F	tdTOM: 53.15±6.35,	tdTOM vs.	T-test	Two-	t[8] =	P =

	ChR2: 75.28±5.77	ChR2		tailed	-2.5784	0.0327
Fig. 3G	Food tdTOM: 75.57±10.50, Novel tdTOM: 1.05±0.31, Food ChR2: 5.66±3.76, Novel ChR2: 62.61±12.05	Food tdTOM vs. Novel tdTOM	Wilcoxon signed rank test	Two-tailed	W = 78	$P^* = 0.0020$
		Food ChR2 vs. Novel ChR2	Wilcoxon signed rank test	Two-tailed	W = 0	$P^* = 0.0313$
		Food tdTOM vs. Food ChR2	Mann-Whitney U test	Two-tailed	U = 170	$P^* = 0.0031$
		Novel tdTOM vs. Novel ChR2	Mann-Whitney U test	Two-tailed	U = 78	$P^* = 0.0009$

*: Bonferroni corrected p-value.

Fig. 4B		Deep vs. Shallow * Time	Repeated measures ANOVA	Tukey-Kramer: Deep vs. Shallow	F(1,399) = 2.7286	$P_{interaction} < 10^{-7}$ $P_{post\text{-}hoc} = 0.1746$
Fig. 4C Max Z-score	6.63±0.65, 6.95±0.88	Deep vs. Shallow	Mann-Whitney U test	Two-tailed	U = 6604	P = 0.8254
Fig. 4C Mean Z-score	0.81±0.54, 1.91±0.57	Deep vs. Shallow	Mann-Whitney U test	Two-tailed	U = 6243	P = 0.0978
Fig. 4E	Off: 30.85±4.25, On: 59.28±7.73	Off vs. On	Wilcoxon signed rank test	Two-tailed	W = 17	$P = 2.9\times10^{-7}$
Fig. 4F pupil	tdTOM: 1.92±0.38, ChR2: 9.15±2.00	tdTOM vs. ChR2	T-test	Two-tailed	T[9] = -3.8985	P = 0.0036
Fig. 4F whisker	tdTOM: 3.11±0.39, ChR2: 7.56±1.05	tdTOM vs. ChR2	Mann-Whitney U test	Two-tailed	U = 21	P = 0.0043
Fig. 4G investig. duration	CNO+tdTOM: 73.33±23.13, CNO+hM4Di: 2.05±0.50	CNO+tdTOM vs. CNO+hM4Di	Mann-Whitney U test	Two-tailed	U = 327	$P = 5.3\times10^{-6}$
Fig. 4G DSP	CNO+tdTOM: 0.59±0.24, CNO+hM4Di: -1.02±0.24	CNO+tdTOM vs. CNO+hM4Di	Mann-Whitney U test	Two-tailed	U = 278	P = 0.0004
Fig. 4H investig. duration	CNO+tdTOM: 127.54±24.15, CNO+hM4Di: 25.26±7.98	CNO+tdTOM vs. CNO+hM4Di	Mann-Whitney U test	Two-tailed	U = 60	P = 0.0009
Fig. 4H DSP	CNO+tdTOM: 0.73±0.19, CNO+hM4Di: -1.34±0.22	CNO+tdTOM vs. CNO+hM4Di	Mann-Whitney U test	Two-tailed	U = 59	P = 0.0020
Fig. 4I	Saline: 23.1±6.2, CNO: 0.00143±0.12	Saline vs. CNO	Wilcoxon signed rank test	Two-tailed	W = 584	$P = 1.1\times10^{-5}$

Fig. 5A MLR firing rate	Off: 8.35±0.72, On: 8.69±0.79	Off vs. On	Wilcoxon signed rank test	Two-tailed	W = 1829	P = 0.0941
Fig. 5A PnO firing rate	Off: 27.81±4.55, On: 31.01±5.08	Off vs. On	Wilcoxon signed rank test	Two-tailed	W = 106	P = 0.0461
Fig. 5A PAG firing rate	Off: 19.51±3.31, On: 14.64±2.21	Off vs. On	Wilcoxon signed rank test	Two-tailed	W = 2281	P = 2.3×10^{-5}
Fig. 5B	tdTOM: 13.90±3.42, MLR: 16.55±4.66, PnO: 7.01±2.29, PAG: 46.94±6.80	MLR vs. tdTOM	T-test	Two-tailed	t[45] = -0.4690	$P^{*} > 0.9999$
		PnO vs. tdTOM	T-test	Two-tailed	t[37] = 1.2786	$P^{*} = 0.6270$
		PAG vs. tdTOM	T-test	Two-tailed	t[55] = -4.1928	$P^{*} = 0.0003$
Fig. 5C	tdTOM: 131.80±14.49, MLR: 126.72±9.80, PnO: 99.74±18.24, PAG: 254.62±30.27	MLR vs. tdTOM	T-test	Two-tailed	t[19] = 0.1650	$P^{*} > 0.9999$
		PnO vs. tdTOM	T-test	Two-tailed	t[19] = 1.0171	$P^{*} = 0.9657$
		PAG vs. tdTOM	T-test	Two-tailed	t[19] = -3.4597	$P^{*} = 0.0079$
Fig. 5D		Deep vs. Shallow * Time	Repeated measures ANOVA	Post-hoc Tukey-Kramer: Deep vs. Shallow	F(1,399) = 2.4720	$P_{interaction} < 10^{-7}$ $P_{post\text{-}hoc} = 0.0015$
Fig. 5E Max Z-score	3.44±0.37, 5.07±0.68	Deep vs. Shallow	Mann-Whitney U test	Two-tailed	U = 1940	P = 0.0401
Fig. 5E Mean Z-score	-0.29±0.31, 1.44±0.44	Deep vs. Shallow	Mann-Whitney U test	Two-tailed	U = 1858	P = 0.0056
Fig. 5F investig. duration	CNO+tdTOM: 58.01±14.82, CNO+hM4Di: 3.54±1.31	CNO+tdTOM vs. CNO+hM4Di	Mann-Whitney U test	Two-tailed	U = 336	P = 8.9×10^{-6}
Fig. 5F DSP	CNO+tdTOM: 0.56±0.27, CNO+hM4Di: -0.42±0.36	CNO+tdTOM vs. CNO+hM4Di	Mann-Whitney U test	Two-tailed	U = 229	P = 0.0393
Fig. 5G investig. duration	CNO+tdTOM: 104.05±24.42, CNO+hM4Di: 31.28±10.30	CNO+tdTOM vs. CNO+hM4Di	Mann-Whitney U test	Two-tailed	U = 86	P = 0.0033

Fig. 5G DSP	CNO+tdTOM: 0.11±0.23, CNO+hM4Di: -1.32±0.24	CNO+tdTOM vs. CNO+hM4Di	Mann-Whitney U test	Two-tailed	U = 85	P = 0.0026

*: Bonferroni corrected p-value.

Fig. 6E investig. duration	tdTOM: 13.90±3.42, PV: 16.38±4.32, SST: 10.99±3.04, TAC1: 58.68±8.43	PV vs. tdTOM	Mann-Whitney U test	Two-tailed	U = 452	$P^* = 0.5628$
		SST vs. tdTOM	Mann-Whitney U test	Two-tailed	U = 537	$P^* > 0.9999$
		TAC1 vs. tdTOM	Mann-Whitney U test	Two-tailed	U = 423	$P^* = 2.7\times10^{-5}$
Fig. 6F	tdTOM: 140.92±17.96, PV: 160.00±42.51, SST: 172.43±40.63, TAC1: 228.68±25.28	PV vs. tdTOM	T-test	Two-tailed	t[15] = -0.4816	$P^* > 0.9999$
		SST vs. tdTOM	T-test	Two-tailed	t[15] = -0.8060	$P^* > 0.9999$
		TAC1 vs. tdTOM	T-test	Two-tailed	t[17] = -2.7811	$P^* = 0.0384$
Fig. 6G DSP	tdTOM: 0.17±0.22, ChR2: 1.07±0.17	tdTOM vs. ChR2	Mann-Whitney U test	Two-tailed	U = 303	P = 0.0001
Fig. 6H investig. Duration	tdTOM: 47.41±13.04, stGtACR2: 5.16±1.12	tdTOM vs. stGtACR2	Mann-Whitney U test	Two-tailed	U = 911	$P = 1.2\times10^{-5}$
Fig. 6I	tdTOM: 140.92±17.96, stGtACR2: 49.21±20.88	tdTOM vs. stGtACR2	Mann-Whitney U test	Two-tailed	U = 183	P = 0.0042

*: Bonferroni corrected p-value.

Table S2. Table of statistics of supplementary figures.

Figure panel	Mean ± s.e.m.	Comparison	Test	Tails or post-hoc test	Test-statistic	P-value
Fig. S2A	Off: 10.04±1.27, On: 18.90±2.12	Off vs. On	Paired t-test	Two-tailed	t[12] = -10.0234	$P = 3.5\times10^{-7}$
Fig. S2B Approach	Familiar tdTOM: 4.52±0.63, Novel tdTOM: 6.07±0.87, Familiar ChR2: 3.62±0.51, Novel ChR2: 7.85±0.92	Familiar ChR2 vs. Novel ChR2	Wilcoxon signed rank test	Two-tailed	W = 91	$P^* = 3.1\times10^{-5}$
		Familiar tdTOM vs. Familiar ChR2	Mann-Whitney U test	Two-tailed	U = 1053	$P^* = 0.5402$
		Novel tdTOM vs. Novel ChR2	Mann-Whitney U test	Two-tailed	U = 855.5	$P^* = 0.8174$
Fig. S2B Sniff	Familiar tdTOM: 1.37±0.26, Novel tdTOM: 3.40±0.71, Familiar ChR2: 0.79±0.10, Novel ChR2: 2.51±0.45	Familiar ChR2 vs. Novel ChR2	Wilcoxon signed rank test	Two-tailed	W = 109	$P^* = 5.5\times10^{-5}$
		Familiar tdTOM vs. Familiar ChR2	Mann-Whitney U test	Two-tailed	U = 1058	$P^* = 0.4903$
		Novel tdTOM vs. Novel ChR2	Mann-Whitney U test	Two-tailed	U = 1050	$P^* = 0.5961$
Fig. S2B Bite	Familiar tdTOM: 1.62±0.76, Novel tdTOM: 10.31±3.02, Familiar ChR2: 4.94±2.21, Novel ChR2: 50.85±5.04	Familiar ChR2 vs. Novel ChR2	Wilcoxon signed rank test	Two-tailed	W = 57	$P^* = 2.4\times10^{-6}$
		Familiar tdTOM vs. Familiar ChR2	Mann-Whitney U test	Two-tailed	U = 864.5	$P^* = 0.8835$
		Novel tdTOM vs. Novel ChR2	Mann-Whitney U test	Two-tailed	U = 533	$P^* = 1.2\times10^{-6}$
Fig. S2B Grab	Familiar tdTOM: 1.30±0.69, Novel tdTOM: 9.85±3.08, Familiar ChR2: 4.68±2.20, Novel ChR2: 49.80±5.12	Familiar ChR2 vs. Novel ChR2	Wilcoxon signed rank test	Two-tailed	W = 47	$P^* = 5.1\times10^{-6}$
		Familiar tdTOM vs. Familiar ChR2	Mann-Whitney U test	Two-tailed	U = 852	$P^* = 0.5428$
		Novel tdTOM vs. Novel ChR2	Mann-Whitney U test	Two-tailed	U = 572	$P^* = 1.1\times10^{-5}$
Fig. S2B Carry	Familiar tdTOM: 0.00±0.00, Novel tdTOM: 0.18±0.09,	Familiar ChR2 vs. Novel ChR2	Wilcoxon signed rank test	Two-tailed	W = 128	$P^* = 0.0002$

	Familiar ChR2: 0.60±0.20, Novel ChR2: 2.20±0.39	Familiar tdTOM vs. Familiar ChR2	Mann-Whitney U test	Two-tailed	U = 784	$P^* = 0.0149$
		Novel tdTOM vs. Novel ChR2	Mann-Whitney U test	Two-tailed	U = 493.5	$P^* < 10^{-7}$
Fig. S2C Sniff to Bite Trans. Prob.	Familiar: 0.30±0.05, Novel: 0.65±0.04	Familiar vs. Novel	Wilcoxon signed rank test	Two-tailed	W = 20	$P^* = 0.0002$

*: Bonferroni corrected p-value.

Fig. S3B Investig. duration	Familiar: 6.33±4.18, Novel: 81.63 ±6.22	Familiar vs. Novel	Wilcoxon signed rank test	Two-tailed	W = 1	P = 0.0002
Fig. S3C Approach	Familiar: 4.43±1.15, Novel: 4.14±0.89	Familiar vs. Novel	Wilcoxon signed rank test	Two-tailed	W = 41.5	P = 0.8633
Fig. S3C Sniff	Familiar: 1.53±0.55, Novel: 1.93±0.34	Familiar vs. Novel	Wilcoxon signed rank test	Two-tailed	W = 41	P = 0.5016
Fig. S3C Bite	Familiar: 4.45±3.58, Novel: 77.74±6.41	Familiar vs. Novel	Wilcoxon signed rank test	Two-tailed	W = 1	P = 0.0002
Fig. S3C Grab	Familiar: 4.12±3.48, Novel: 76.68±6.51	Familiar vs. Novel	Wilcoxon signed rank test	Two-tailed	W = 1	P = 0.0002
Fig. S3C Carry	Familiar: 0.35±0.27, Novel: 1.95±0.35	Familiar vs. Novel	Wilcoxon signed rank test	Two-tailed	W = 11	P = 0.0067

Fig. S4A Novel cricket	Familiar: 6.34±2.30, Novel: 55.56±4.92, Novel cricket: 69.53±12.54	Familiar vs. Novel Cricket	Mann-Whitney U test	Two-tailed	U = 914	$P^* = 0.0007$
		Novel vs. Novel Cricket	Mann-Whitney U test	Two-tailed	U = 993	$P^* = 0.5369$
Fig. S4B Moving static	Familiar: 0.02±0.02, Novel: 94.08±7.52	Familiar moving vs. Novel static	Wilcoxon signed rank test	Two-tailed	W = 0	P = 0.0020
Fig. S4C Dead cricket	Familiar: 10.17±4.13, Novel: 72.54±7.26	Familiar dead cricket vs. Novel	Wilcoxon signed rank test	Two-tailed	W = 23	P = 0.0001

*: Bonferroni corrected p-value.

Fig. S5C Investig. duration	Familiar: 67.08±11.00, Novel: 9.62 ±5.04	Familiar Food vs. Novel Object	Wilcoxon signed rank test	Two-tailed	W = 28	P = 0.0156
Fig. S5D Approach	Familiar: 3.57±1.13, Novel: 3.28±0.92	Familiar Food vs. Novel	Wilcoxon signed rank	Two-tailed	W = 9	P = 0.8750

		Object	test			
Fig. S5D Sniff	Familiar: 0.68±0.21, Novel: 0.79±0.38	Familiar Food vs. Novel Object	Wilcoxon signed rank test	Two-tailed	W = 16	P = 0.8125
Fig. S5D Bite	Familiar: 65.85±10.96, Novel: 8.39±4.73	Familiar Food vs. Novel Object	Wilcoxon signed rank test	Two-tailed	W = 28	P = 0.0156
Fig. S5D Grab	Familiar: 51.70±12.96, Novel: 8.11±4.65	Familiar Food vs. Novel Object	Wilcoxon signed rank test	Two-tailed	W = 21	P = 0.0313
Fig. S5D Carry	Familiar: 0.54±0.37, Novel: 0.44±0.44	Familiar Food vs. Novel Object	Wilcoxon signed rank test	Two-tailed	W = 2	P > 0.9999

Fig. S6A	Off: 31.89±5.74, On: 27.31±5.14	Off vs. On	Wilcoxon signed rank test	Two-tailed	W = 104	P = 0.0002
Fig. S6B Approach	Familiar tdTOM: 12.72±1.66, Novel tdTOM: 15.15±1.58, Familiar stGtACR2: 5.89±1.17, Novel stGtACR2: 7.17±1.36	Familiar stGtACR2 vs. Novel stGtACR2	Wilcoxon signed rank test	Two-tailed	W = 90.5	P^* = 0.4388
		Familiar tdTOM vs. Familiar stGtACR2	Mann-Whitney U test	Two-tailed	U = 1238	P^* = 0.0011
		Novel tdTOM vs. Novel stGtACR2	Mann-Whitney U test	Two-tailed	U = 1247	P^* = 0.0006
Fig. S6B Sniff	Familiar tdTOM: 3.17±0.33, Novel tdTOM: 6.92±0.71, Familiar stGtACR2: 2.16±0.49, Novel stGtACR2: 4.12±0.76	Familiar stGtACR2 vs. Novel stGtACR2	Wilcoxon signed rank test	Two-tailed	W = 38	P^* = 0.0008
		Familiar tdTOM vs. Familiar stGtACR2	Mann-Whitney U test	Two-tailed	U = 1180	P^* = 0.0203
		Novel tdTOM vs. Novel stGtACR2	Mann-Whitney U test	Two-tailed	U = 1190	P^* = 0.0130
Fig. S6B Bite	Familiar tdTOM: 3.67±1.63, Novel tdTOM: 40.04±12.78, Familiar stGtACR2: 0.88±0.41, Novel stGtACR2: 2.92±1.20	Familiar stGtACR2 vs. Novel stGtACR2	Wilcoxon signed rank test	Two-tailed	W = 17	P^* = 0.0146
		Familiar tdTOM vs. Familiar stGtACR2	Mann-Whitney U test	Two-tailed	U = 1067	P^* = 0.7133
		Novel tdTOM vs. Novel stGtACR2	Mann-Whitney U test	Two-tailed	U = 778	P^* = 7.0×10^{-6}
Fig. S6B Grab	Familiar tdTOM: 3.49±1.62, Novel tdTOM: 39.14±13.16,	Familiar stGtACR2 vs. Novel stGtACR2	Wilcoxon signed rank test	Two-tailed	W = 1	P^* = 0.0117

	Familiar stGtACR2: 0.52±0.36, Novel stGtACR2: 1.72±1.09	Familiar tdTOM vs. Familiar stGtACR2	Mann-Whitney U test	Two-tailed	U = 1121	0.0553 $P^* = 1.1\times10^{-7}$
		Novel tdTOM vs. Novel stGtACR2	Mann-Whitney U test	Two-tailed	U = 1364	
Fig. S6B Carry	Familiar tdTOM: 0.11±0.08, Novel tdTOM: 0.45±0.15, Familiar stGtACR2: 0.03±0.03, Novel stGtACR2: 0.13±0.10	Familiar stGtACR2 vs. Novel stGtACR2	Wilcoxon signed rank test	Two-tailed	W = 0	$P^* > 0.9999$ $P^* > 0.9999$ $P^* = 0.1751$
		Familiar tdTOM vs. Familiar stGtACR2	Mann-Whitney U test	Two-tailed	U = 1006	
		Novel tdTOM vs. Novel stGtACR2	Mann-Whitney U test	Two-tailed	U = 1077	
Fig. S6B Avoid	Familiar tdTOM: 0.03±0.03, Novel tdTOM: 0.03±0.03, Familiar stGtACR2: 00.00±00.00, Novel stGtACR2: 0.10±0.07	Familiar stGtACR2 vs. Novel stGtACR2	Wilcoxon signed rank test	Two-tailed	W = 0	$P^* > 0.9999$ $P^* > 0.9999$ $P^* > 0.9999$
		Familiar tdTOM vs. Familiar stGtACR2	Mann-Whitney U test	Two-tailed	U = 1006	
		Novel tdTOM vs. Novel stGtACR2	Mann-Whitney U test	Two-tailed	U = 974	
Fig. S6C Sniff to Bite Trans. Prob.	Familiar: 0.11±0.07, Novel: 0.21±0.07	Familiar vs. Novel	Wilcoxon signed rank test	Two-tailed	W = 10	P = 0.1563
Fig. S6D Traveled dist.	tdTOM: 1257.60±175.00, stGtACR2: 1337.80±196.11	tdTOM vs. stGtACR2	T-test	Two-tailed	t[9] = -0.2989	P = 0.7718
Fig. S6E investig. duration	CNO+tdTOM: 52.57±13.04, CNO+hM4Di: 3.96±2.19	CNO+tdTOM vs. CNO+hM4Di	Mann-Whitney U test	Two-tailed	U = 83	P = 0.0006
Fig. S6F DSP	CNO+tdTOM: 0.75±0.15, CNO+hM4Di: -1.01±0.38	CNO+tdTOM vs. CNO+hM4Di	Mann-Whitney U test	Two-tailed	U = 73	P = 0.0052

*: Bonferroni corrected p-value.

Fig. S7B investig. duration	tdTOM: 23.30±3.73, ChR2: 60.25±10.62, stGtACR2: 7.02±1.74	tdTOM vs. ChR2	Mann-Whitney U test	Two-tailed	U = 191.5	$P^* = 0.0055$
		tdTOM vs. stGtACR2	Mann-Whitney U test	Two-tailed	U = 380	$P^* = 0.0003$
Fig. S7C	tdTOM: 69.09±8.15,	tdTOM vs.	Mann-	Two-	U = 205.5	$P^* =$

investig. duration	ChR2: 100.70±6.77, stGtACR2: 11.16±2.23	ChR2	Whitney U test	tailed		0.0321
		tdTOM vs. stGtACR2	Mann-Whitney U test	Two-tailed	U = 397	$P^{*} = 2.3\times10^{-5}$
Fig. S7E investig. duration	CNO+tdTOM: 148.36±48.31, CNO+hM4Di: 41.20±23.83	CNO+tdTOM vs. CNO+hM4Di	T-test	Two-tailed	t[2] = -0.2989	P = 0.0499
Fig. S7F DSP	CNO+tdTOM: 0.67±0.34, CNO+hM4Di: -1.40±0.17	CNO+tdTOM vs. CNO+hM4Di	T-test	Two-tailed	t[2] = 7.4814	P = 0.0174

*: Bonferroni corrected p-value.

Fig. S9A Mean Z-score	Shoallow: 0.78±0.26, Deep: 4.10±0.53	Shallow vs. Deep	Mann-Whitney U test	Two-tailed	U = 130003	$P < 10^{-7}$
Fig. S9B Mean Z-score	Shoallow: 1.02±0.32, Deep: 3.96±1.35	Shallow vs. Deep	Mann-Whitney U test	Two-tailed	U = 1890	P = 0.0178
Fig. S9C Mean Z-score	Deep/object: 4.10±0.53, Deep-like/food: 0.38±0.69	Deep/object vs. Deep-like/food	Mann-Whitney U test	Two-tailed	U = 1774	P = 0.0156

Fig. S10E Pupil size	Before investigation: 20.81±0.93, During investigation: 24.38±0.91	Before investigation vs. During investigation	Paired t-test	Two-tailed	t[8] = -2.6549	P = 0.0290

Fig. S11C Number of returns to nose poke	Opto nose poke: 106.66±19.67, Nose None-opto nose poke: 673.00±178.98	tdTOM vs. ChR2	Paired t-test	Two-tailed	t[4] = -3.1453	P = 0.0347

Fig. S13A DSP object	tdTOM: 0.17±0.22, ChR2: 0.68±0.21	tdTOM vs. ChR2	Mann-Whitney U test	Two-tailed	U = 442	P = 0.0133
Fig. S13B DSP social	tdTOM: -0.38±0.19, ChR2: 0.57±0.36	tdTOM vs. ChR2	Mann-Whitney U test	Two-tailed	U = 179.5	P = 0.0167

Fig. S14A pupil	tdTOM: 1.92±0.38, ChR2: 1.17±0.99	tdTOM vs. ChR2	T-test	Two-tailed	t[7] = 0.8676	P = 0.4143
Fig. S14A	tdTOM: 3.11±0.39, ChR2: 2.38±0.49	tdTOM vs. ChR2	T-test	Two-tailed	t[7] = 1.1042	P = 0.3060

whisker						
Fig. S14B pupil	tdTOM: 1.92±0.38, ChR2: 1.50±0.59	tdTOM vs. ChR2	T-test	Two-tailed	t[7] = 0.6052	P = 0.5641
Fig. S14B whisker	tdTOM: 3.11±0.39, ChR2: 3.12±0.27	tdTOM vs. ChR2	T-test	Two-tailed	t[7] = -0.0345	P = 0.9734
Fig. S14C pupil	tdTOM: 1.92±0.38, ChR2: 7.01±2.02	tdTOM vs. ChR2	T-test	Two-tailed	t[9] = -2.7200	P = 0.0225
Fig. S14C whisker	tdTOM: 3.11±0.39, ChR2: 7.71±1.48	tdTOM vs. ChR2	T-test	Two-tailed	t[9] = -3.2851	P = 0.0095

Fig. S16A DSP social	tdTOM: -0.12±0.20, ChR2: 0.62±0.10, stGtACR2: -1.16±0.19	tdTOM vs. ChR2	unequal variances t-test	Two-tailed	t[16.6175] = -3.2713	P^* = 0.0092
		tdTOM vs. stGtACR2	Mann-Whitney U test	Two-tailed	U = 168	P^* = 0.0266
Fig. S16B DSP object	tdTOM: 0.51±0.13, stGtACR2: -0.64±0.20	tdTOM vs. stGtACR2	Mann-Whitney U test	Two-tailed	U = 1195	P = 7.7×10^{-5}

*: Bonferroni corrected p-value.

Fig. S17A object investig. duration	GAD2 familiar: 6.34±2.30, GAD2 novel: 55.56±4.92, TAC1 familiar: 4.77±1.52, TAC1 novel: 58.68±8.43	GAD2 familiar vs. TAC1 familiar	Mann-Whitney U test	Two-tailed	U = 1202	P^* = 0.6686
		GAD2 novel vs. TAC1 novel	Mann-Whitney U test	Two-tailed	U = 1243	P^* > 0.9999
Fig. S17B social invest. duration	GAD2: 239.16±21.52, TAC1: 228.68±25.28	GAD2 vs. TAC1	T-test	Two-tailed	t[17] = 0.2898	P = 0.7755

*: Bonferroni corrected p-value.

Fig. S18A pupil	tdTOM: 1.92±0.38, ChR2: 6.26±1.12	tdTOM vs. ChR2	T-test	Two-tailed	t[9] = -3.9523	P = 0.0033
Fig. S18B whisker	tdTOM: 3.11±0.39, ChR2: 6.69±0.48	tdTOM vs. ChR2	T-test	Two-tailed	t[9] = -5.8929	P = 0.0002

Movie S1.
Example of interaction of a wild-type mouse with familiar and novel objects.

Movie S2.
Example of interaction of a mouse with objects during photo-activation of ZIm^{GAD2}.

Movie S3.
Example of interaction of a mouse with objects during photo-activation of ZIm^{GAD2} in an FADC test with 4 familiar objects and 1 novel object.

Movie S4.
Example of interaction of a mouse with a novel object and a familiar food pellet during photo-activation of ZIm^{GAD2}.

Movie S5.
Example of interaction of a mouse with a novel moving object and familiar cricket during photo-activation of ZIm^{GAD2}.

Movie S6.
Example of interaction of a mouse with objects during photo-inhibition of ZIm^{GAD2}.

Movie S7.
Example of interaction of a mouse with a conspecific intruder during photo-activation of ZIm^{GAD2}.